Biomarker Accessible and Chemically Addressable Mechanistic Subtypes of BRAF Melanoma

Banu Eskiocak[1], Elizabeth A. McMillan[1], Saurabh Mendiratta[1], Rahul K. Kollipara[2], Hailei Zhang[3], Caroline G. Humphries[2], Changguang Wang[4], Jose Garcia-Rodriguez[4], Ming Ding[4], Aubhishek Zaman[1], Tracy I. Rosales[1], Ugur Eskiocak[5], Michael P. Smith[6], Jessica Sudderth[5], Kakajan Komurov[7], Ralph J. Deberardinis[5], Claudia Wellbrock[6], Michael A. Davies[8], Jennifer A. Wargo[9,10], Yonghao Yu[4], Jef K. De Brabander[4], Noelle S. Williams[4], Lynda Chin[10], Helen Rizos[11], Georgina V. Long[11], Ralf Kittler[2], and Michael A. White[1]

ABSTRACT

Genomic diversity among melanoma tumors limits durable control with conventional and targeted therapies. Nevertheless, pathologic activation of the ERK1/2 pathway is a linchpin tumorigenic mechanism associated with the majority of primary and recurrent disease. Therefore, we sought to identify therapeutic targets that are selectively required for tumorigenicity in the presence of pathologic ERK1/2 signaling. By integration of multigenome chemical and genetic screens, recurrent architectural variants in melanoma tumor genomes, and patient outcome data, we identified two mechanistic subtypes of $BRAF^{V600}$ melanoma that inform new cancer cell biology and offer new therapeutic opportunities. Subtype membership defines sensitivity to clinical MEK inhibitors versus TBK1/IKBKε inhibitors. Importantly, subtype membership can be predicted using a robust quantitative five-feature genetic biomarker. This biomarker, and the mechanistic relationships linked to it, can identify a cohort of best responders to clinical MEK inhibitors and identify a cohort of TBK1/IKBKε inhibitor–sensitive disease among nonresponders to current targeted therapy.

SIGNIFICANCE: This study identified two mechanistic subtypes of melanoma: (1) the best responders to clinical BRAF/MEK inhibitors (25%) and (2) nonresponders due to primary resistance mechanisms (9.9%). We identified robust biomarkers that can detect these subtypes in patient samples and predict clinical outcome. TBK1/IKBKε inhibitors were selectively toxic to drug-resistant melanoma. *Cancer Discov; 7(8); 832–51. ©2017 AACR.*

See related commentary by Jenkins and Barbie, p. 799.

[1]Department of Cell Biology, The University of Texas Southwestern Medical Center, Dallas, Texas. [2]Eugene McDermott Center for Human Growth and Development, The University of Texas Southwestern Medical Center, Dallas, Texas. [3]The Broad Institute of Harvard and Massachusetts Institute of Technology, Cambridge, Massachusetts. [4]Department of Biochemistry, The University of Texas Southwestern Medical Center, Dallas, Texas. [5]Children's Research Institute and the Department of Pediatrics, The University of Texas Southwestern Medical Center, Dallas, Texas. [6]Manchester Cancer Research Centre, Wellcome Trust Centre for Cell-Matrix Research, The University of Manchester, Manchester, United Kingdom. [7]Division of Biomedical Informatics, Cincinnati Children's Hospital Medical Center, Cincinnati, Ohio. [8]Department of Melanoma Medical Oncology, The University of Texas MD Anderson Cancer Center, Houston, Texas. [9]Department of Surgical Oncology, The University of Texas MD Anderson Cancer Center, Houston, Texas. [10]Department of Genomic Medicine, The University of Texas MD Anderson Cancer Center, Houston, Texas. [11]Melanoma Institute, University of Sydney, Sydney, New South Wales, Australia.

Note: Supplementary data for this article are available at Cancer Discovery Online (http://cancerdiscovery.aacrjournals.org/).

Corresponding Author: Michael A. White, The University of Texas Southwestern Medical Center, 6000 Harry Hines Boulevard, Dallas, TX 75390-9039. Phone: 214-648-2861; Fax: 214-648-8694; E-mail: michael.white@utsouthwestern.edu

doi: 10.1158/2159-8290.CD-16-0955

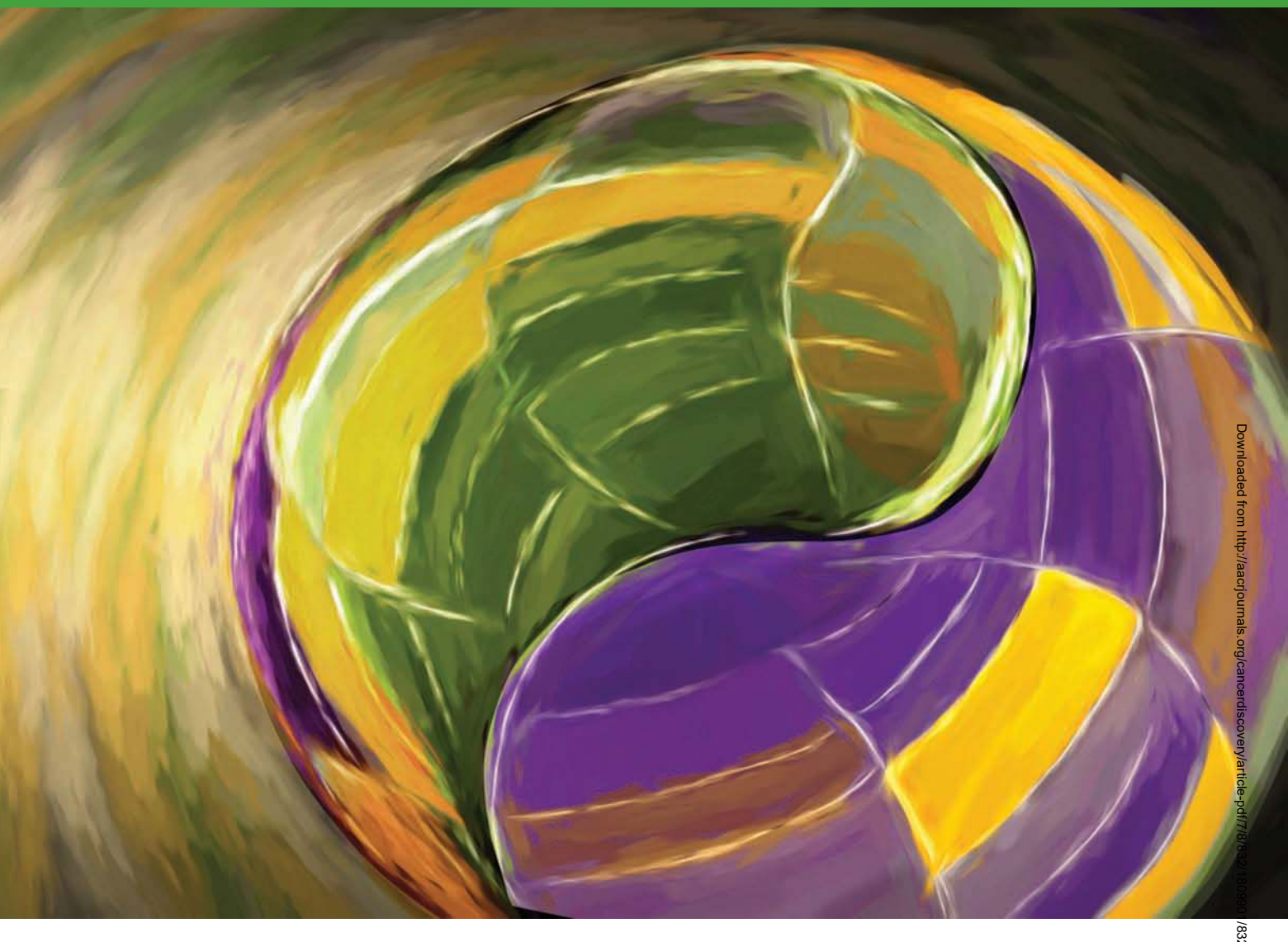

INTRODUCTION

Despite displaying the greatest mutational diversity of any neoplastic disease (1, 2), fully half of all cutaneous melanomas harbor gain-of-function alleles in the *BRAF* proto-oncogene (3, 4). In consequence, direct pharmacologic inhibition of the most common of these variants, $BRAF^{V600}$, has become a translational exemplar for targeted therapy (5). A rapid series of advances have demonstrated both exceptional initial patient response and ready emergence of therapy-resistant disease. Identified resistance mechanisms include gain-of-function mutations in *NRAS* (6), *MAP2K1* (7, 8), and *PIK3CA* (9); amplification of *COT* (10); upregulation of PDGFRβ (6), EGFR (11–13), ERBB3 (14), and IGFR1 (15); and amplification (16) or alternative splice variant expression (17) of *BRAF*. The majority of these resistance mechanisms appear to be a consequence of $BRAF^{V600}$-independent MAPK pathway activation. To defend against this, many current clinical and translational efforts are focused on chemical inhibition of the protein kinases MEK1/2 and ERK1/2 that mediate $BRAF^{V600}$-induced tumorigenicity (18). However, the absence of common disease-specific alleles requires targeting of wild-type (WT) proteins commonly engaged to support normal tissue homeostasis. This leads to the conundrum of dose-limiting toxicity, which can narrow the therapeutic window and limit patient benefit (19). Melanoma-selective vulnerabilities within the ERK1/2 regulatory network may offer themselves as additional target opportunities; however, the diversity and cryptic pharmacologic accessibility of this regulatory network is a considerable challenge confronting that approach. Remarkable advances in tolerance-breaking immune modulation may lead to effective therapy that is agnostic to BRAF-mutant status and MAPK pathway activation, but this will clearly be aided by collaborating interventions that directly target tumor tissue (20–25).

As an alternative approach for nomination of melanoma cell–autonomous intervention targets, we considered opportunities associated with collateral mechanistic liabilities that arise as a consequence of pathologic MAPK pathway activation. If detectable and actionable, targeting these liabilities would be expected to be synthetic-lethal to any and all of the myriad genomic alterations that lead to tumorigenic

dysregulation of the MAPK regulatory network. A tiered multigenomic RNAi-mediated screening strategy coupled to molecular correlates in human tumor tissues, patient outcome data, and consideration of 130 drugs and investigational chemical compounds uncovered two mechanistic subtypes of melanoma. These subtypes are simultaneously detectable with a robust quantitative biomarker and actionable through distinct chemical vulnerabilities. A SOX10-addicted subtype specifies $BRAF^{V600}$ melanomas that are intrinsically sensitive to clinical MEK inhibitors irrespective of sensitivity or resistance to clinical $BRAF^{V600}$ inhibitors, is detectable in approximately 25% of the population of patients with $BRAF^{V600}$ melanoma, and was validated in three independent patient cohorts on two continents. Characterization of the direct SOX10 transcriptional network in this subtype delivered previously unknown lineage-specific, tumor-activated proteins required for matrix-independent colony growth and defined discrete protumorigenic transcriptional programs collaboratively controlled by SOX10 together with MITF. An "innate immune" subtype specifies $BRAF^{V600}$ and $BRAF^{WT}$ melanomas that are intrinsically resistant to clinical MEK and BRAF inhibitors, and is detectable in approximately 9.9% of melanomas. Unbiased virtual and empirical chemical screening efforts identified low nanomolar TBK1/IKKε inhibitors, validated by four different chemical scaffolds, as lead compounds that are selectively toxic in these otherwise targeted therapy–resistant melanomas *in vitro* and *in vivo*. The mechanism of action appears to be through inhibition of TBK1/IKKε-dependent Hippo pathway suppression and AKT pathway activation in this subtype. A key mechanistic determinant of subtype membership was determined to be nicotinamide N-methyltransferase (NNMT)–dependent chromatin organization. These findings contribute to productive genomics-guided medicine both by predicting the best responders to currently available BRAF/MEK-targeted agents and by nominating TBK1/IKKε inhibition as a therapy for an important BRAF/MEK targeted therapy–resistant subtype.

RESULTS

Integrative Analysis of Functional Genomics and Copy-Number Variation in Melanoma Cells and Tissues

To help identify clinically relevant intervention targets in melanoma from cell-based screening efforts, we combined genome-wide RNAi toxicity screens in melanoma cell lines with corresponding detection of genomic copy-number gain in melanoma tumors. We reasoned that gene products commonly participating in bona fide context-specific support of melanoma cell survival would likely be the subjects of selective pressure for gain-of-expression genomic alterations during human tumor initiation and progression.

An extensive combined experimental and computational analysis among 19 melanoma cell lines, 3 telomerase immortalized nontumorigenic cell strains, and 106 tumors returned *KPNB1, TPX2, BRAF, GOLPH3, SOX10, METTL18, UBE2Z, CEP68, MARCH6, LRP12, ZNF706, ZC3H7B, ATXN10, COG5, MTX1,* and *ZNF79* as candidate copy number–driven melanoma cell survival genes (Supplementary Fig. S1A–S1R and Supplementary Fig. S2A–S2C; Supplementary Tables S1–S5). Among these, the lineage-specific transcription factor SOX10 displayed the largest expression variation among cell lines and tumor samples, which was significantly correlated with *SOX10* gene copy number (Supplementary Fig. S3A, $P = 0.0006$) and *SOX10* siRNA sensitivity (Supplementary Fig. S3B–S3L, Mann–Whitney $P < 0.0001$). Furthermore, SOX10 has recently been demonstrated to support melanoma initiation in mice (26). Thus, in addition to MITF (27), SOX10 presents itself as a likely lineage-selective, copy-number–driven oncogene in human melanoma. Therefore, we experimentally defined cancer-associated SOX10 target genes using a combination of SOX10 chromatin immunoprecipitation sequencing (ChIP-seq), whole-genome transcript analysis ± SOX10 expression, and SOX10 coexpression correlation analysis in tumors from three independent melanoma patient cohorts. Six of 25 of the resulting gene candidates made significant contributions to anchorage-independent melanoma cancer cell colony formation (Supplementary Fig. S3M–S3R), suggesting a highly combinatorial contribution of SOX10 target genes to tumorigenic propensity. Notably, these included the type 1 Charcot–Marie–Tooth disease gene *GJB1* (28); the melanoma metastasis prognostic indicator, *CEACAM1* (29, 30); and the BRAF therapy resistance gene *ERBB3* (ref. 14; Supplementary Fig. S3R–S3V; Supplementary Tables S6–S11).

SOX10 Addiction Specifies Sensitivity of BRAF-Mutant Melanomas to BRAF and MEK Inhibitors *In Vitro* and in Patients

SOX10 suppression has been reported to be associated with resistance to BRAF-targeted therapy in melanoma, at least in part as a consequence of increased TGFβ receptor 2 (TGFBR2) expression (12). Indeed, we found that TGFBR2 expression is likely directly suppressed by SOX10 occupancy of *TGFBR2* gene regulatory elements (Supplementary Fig. S3M; Supplementary Tables S6–S8; SOX10 ChIP-seq and Supplementary Table S9; whole-transcriptome analysis ± SOX10 depletion, Supplementary Table S10). This prompted us to examine the correlation of SOX10 addiction with *BRAF* mutation status and response to clinical BRAF and MEK inhibitors. Oncogenic *BRAF* mutations were present in both SOX10-dependent and SOX10-independent melanoma cell lines (Fig. 1A). However, SOX10-dependent cell lines were sensitive to the MEK inhibitor trametinib, whereas SOX10-independent cell lines were uniformly resistant to both trametinib and the mutant BRAF inhibitor (BRAFi) vemurafenib irrespective of BRAF-mutant status (Fig. 1B and C). The opportunity to potentially discriminate cancer cell sensitivity to BRAF/MEK pathway inhibition, based on the biological context underpinning SOX10 addiction, motivated us to search for molecular biomarkers associated with these phenotypes. To do that, we employed a regularized linear regression algorithm to help identify distinct gene expression features from whole-genome transcript profiles that may be predictive of response to depletion of SOX10 (31–34). A 5-gene solution was returned that was quantitatively associated with SOX10 addiction (Fig. 1A). We then calculated the linear weighted sums of the individual expression values for each feature in the expression biomarker, for each cell line, by multiplying the indicated Log_2 Illumina signal intensity values with

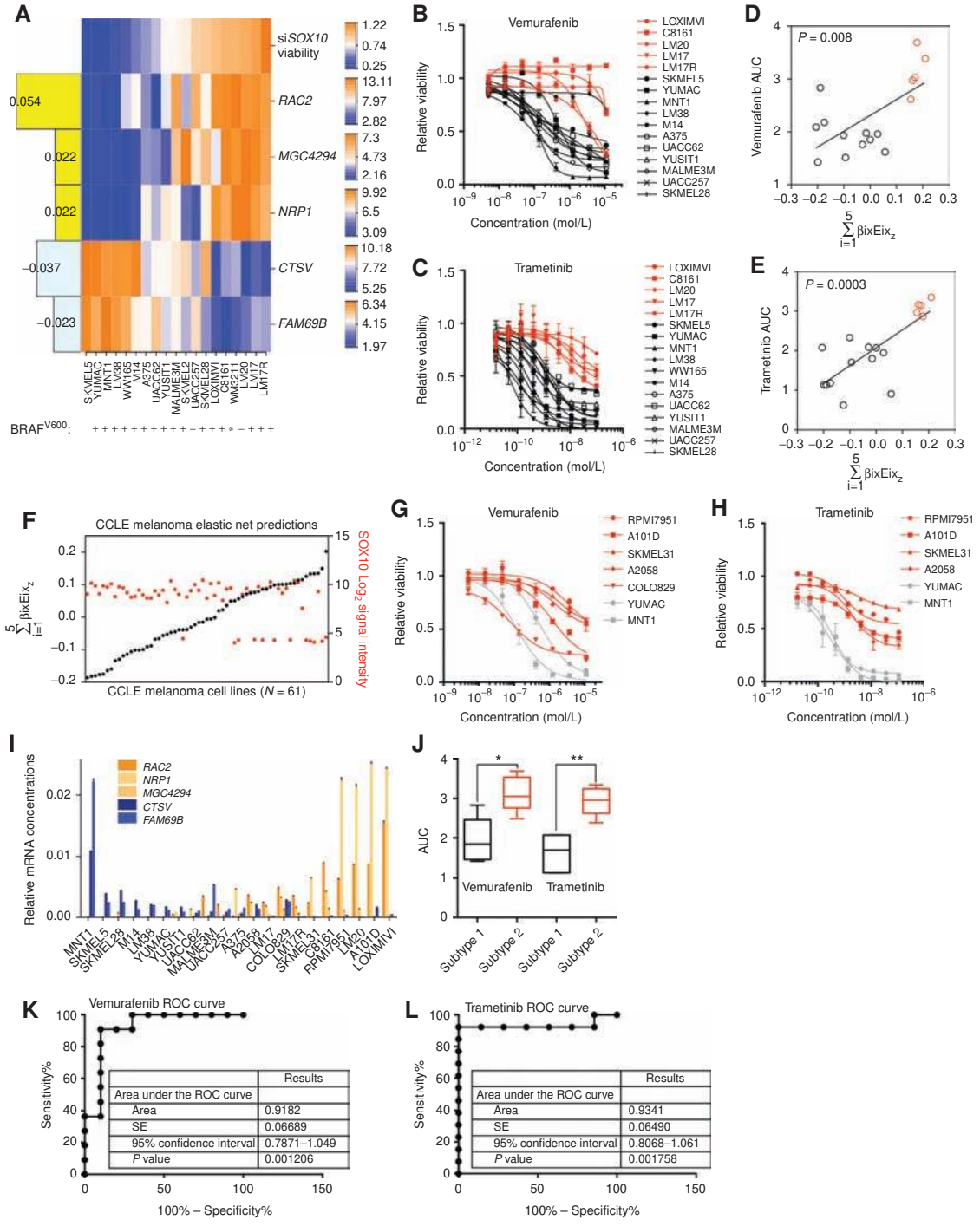

Figure 1. SOX10 addiction specifies sensitivity of BRAF-mutant melanomas to BRAF and MEK inhibitors *in vitro*. **A,** A sparse linear regression model (elastic net) for weighted expression features that specify SOX10 dependence or independence. siRNA response is indicated as a heat map (top row). The central heat map indicates predictive gene expression features (values are $\log_2$) across the indicated cell lines. Bar plot on the left indicates the average weight for the corresponding feature as determined from a 100× bootstrapping analysis. Vemurafenib (**B**) and trametinib (**C**) dose–response curves for SOX10-dependent (black) and SOX10-independent (red) cell lines. Dots indicate mean ± SD ($n = 3$). Linear regression analysis of vemurafenib (**D**) and trametinib (**E**) AUC values for each cell line in the melanoma panel and the prediction scores determined using a summed weight metric based on the elastic net–derived expression features. **F,** Distribution of CCLE melanoma cell lines based on the linear weighted sums of the individual gene expression values for each predictive feature (left *y*-axis) and the corresponding SOX10 $\log_2$ signal intensity values from microarray is also shown (right *y*-axis). Vemurafenib (**G**) and trametinib (**H**) dose–response curves for predicted targeted therapy–resistant melanoma cell lines (red) and the previously tested targeted therapy–sensitive cell lines (gray, as comparison). **I,** qPCR analysis of *RAC2, NRP1, MGC4294, CTSV,* and *FAM69B* mRNA concentrations in melanoma cells. Bars indicate mean ± SD ($n = 3$). **J,** Comparison of AUC values for dose–response curves from predicted targeted therapy–sensitive (subtype 1) and –resistant (subtype 2) melanoma cell lines exposed to vemurafenib (two-sided unpaired Mann–Whitney test; *, $P = 0.0159$) and trametinib (two-sided unpaired Mann–Whitney test; **, $P = 0.0079$). **K** and **L,** ROC curve analysis for vemurafenib (**K**) and trametinib (**L**) response.

the weights determined by the elastic net analysis (Fig. 1A). Negative linear weighted sum value for a cell line indicates predicted sensitivity to BRAF and MEK inhibitors, due to the negative weight values associated with *CTSV* and *FAM69B* genes, whereas positive linear weighted sum values indicate predicted resistance to BRAF and MEK inhibitors due to the positive weight values associated with *RAC2, MGC4294,* and *NRP1* genes (Fig. 1A, weights are indicated on the left side of the biomarker gene expression). The linear weighted sums of the individual expression values for each feature in the expression biomarker, for each cell line, showed significant correlation with vemurafenib and trametinib LD_{50} (Supplementary Fig. S4A and S4B) and log kill as determined by AUC (Fig. 1D and E), suggesting potential utility of this metric as a prediction score for response to targeted therapy. To test the predictive utility of the biomarker outside of the "discovery" cell line panel, we rank-ordered the 61 melanoma cell lines from the Cancer Cell Line Encyclopedia (CCLE) according to the available Affymetrix-derived individual expression values for each biomarker feature (*RAC2, NRP1, MGC4294, CTSV,* and *FAM69B*; Fig. 1F; Supplementary Fig. S4C; Supplementary Table S12). Five publicly accessible $BRAF^{V600E}$ cell lines present in the predicted-resistant tail of the distribution (cell lines with the positive linear weighted sum values toward the right side of the distribution) were tested, and 4 of these were found to be vemurafenib and trametinib resistant (Fig. 1G and H). Among the predictive expression features, we found that sensitivity to depletion of RAC2 specifically correlated with SOX10 independence (blue bars), suggesting discrete mechanistic contributions of SOX10 and RAC2 to the targeted therapy–sensitive versus targeted therapy–resistant classes (Supplementary Fig. S4D). Of note, SOX10 expression alone was not sufficient to predict targeted therapy resistance (Fig. 1F, SOX10 signal intensity), emphasizing the utility of the elastic net–derived feature set to predict the response of melanoma tumor cells to targeted therapy.

To assess biomarker performance using discrete measurements of biomarker gene expression, as opposed to whole-genome transcript profiles, qPCR was employed across the cell line panel (Fig. 1I). The qPCR values were then used to assign a prediction score (summed weighted expression) to each cell line (Supplementary Fig. S4E). The samples in the tails of the score distribution [5 lowest (MNT1, SKMEL5, SKMEL28, M14, and LM38) and 5 highest (C8161, RPMI7951, LM20, A101D, and LOXIMVI)] corresponded to significant differences in drug sensitivity in the directions predicted by their biomarker scores (Fig. 1J). In addition, a two-class comparison of predicted versus measured response to targeted therapy was utilized across the cell panel using ROC. Following standard protocol, true-positive values (sensitivity%) were plotted as a function of the false-positive rate (100%-specificity%) for each threshold of the prediction score. The resulting ROC curves showed significant AUC, which is a measure of the strength of the prediction score to discriminate BRAF/MEK inhibitor–sensitive versus –resistant melanoma cells (Fig. 1K and L).

The magnitude of the separation of sensitivity of these cell lines to BRAF pathway inhibition prompted us to ask if the quantitative expression features associated with SOX10 addiction could discriminate patient responses to BRAF- and/or MEK-targeted therapy. To test this, we first leveraged a clinical study with whole-genome transcript profiles derived from resected tumors from 30 patients with $BRAF^{V600}$-mutant melanoma undergoing treatment with the $BRAF^{V600}$ inhibitors dabrafenib or vemurafenib (35). The multifeature expression biomarker was used to assign probability values for membership of each patient in the SOX10-addicted (vemurafenib/trametinib sensitive) class or the SOX10-independent (vemurafenib/trametinib resistant) class. Given the on/off nature of the expression of the biomarker genes in the cell lines associated with these classes (Fig. 1A; Supplementary Fig. S4C), we again employed a summed-weight metric (linear weighted sums of the gene expression of each feature in the biomarker) to rank the patients based on the expression values of the biomarker genes in the patients' tumors (Fig. 2A; Supplementary Table S12). A survival analysis, comparing the quartiles from the extrema of the resulting ranked distribution (< −0.05 vs. >0.05, Fig. 2A; Supplementary Table S12), revealed a marked separation in patient outcome—with membership in the "vemurafenib/trametinib-resistant" class predictive of poor prognosis (Fig. 2B). Importantly, this result was reproducible in an independent cohort of patients who received $BRAF^{V600}$ inhibitors (dabrafenib or vemurafenib) or a combination of $BRAF^{V600}$ and MEK inhibitor (dabrafenib and trametinib) therapy (Fig. 2C and D; Supplementary Table S13). This outcome association is especially notable, as membership in the "vemurafenib/trametinib-resistant" class corresponds to better prognosis in patients treated with standard chemotherapy in two independent cohorts (Supplementary Fig. S5A and S5B; Supplementary Table S12; ref. 36). Finally, we analyzed a third independent cohort that reported best overall response in patients undergoing $BRAF^{V600}$ (dabrafenib or vemurafenib) or combination of $BRAF^{V600}$ and MEK inhibitor (dabrafenib and trametinib) therapy, and was associated with RNA-sequencing (RNA-seq) transcript profiles derived from melanoma tumors isolated prior to therapy (ref. 37; Fig. 2E). As this cohort was too small to select the tails of the sample score distribution, we resorted to dichotomization of the patients into two groups of equal size based on the summed-weight metric (Fig. 2E; Supplementary Table S12). Nevertheless, we still observed a significant enrichment of poor responders in the predicted-resistant group (Fig. 2F). Together, these observations support the notion that the cellular SOX10 addiction–derived quantitative multifeature biomarker can detect distinct mechanistic subtypes of melanoma that correspond to intrinsic sensitivity or resistance to $BRAF^{V600}$/MEK-targeted therapy.

To examine if the expression biomarker may also report acquired resistance, we obtained tumor biopsies from patients before and during the course of targeted MAPK pathway therapy. Again, individual gene features were measured by qPCR and used to calculate a predicted response score. We found that 4 of 4 patients with an initial "targeted therapy–sensitive" score progressed to a "resistant" score on therapy. Moreover, the prediction score did not change in 2 of 2 patients whose initial signature was already in the "targeted therapy–resistant" class (Fig. 2G). Similar observations were made using an *in vitro* model of acquired resistance to trametinib consisting of a trametinib-sensitive A375 parental line and selection-derived trametinib-resistant A375 cell

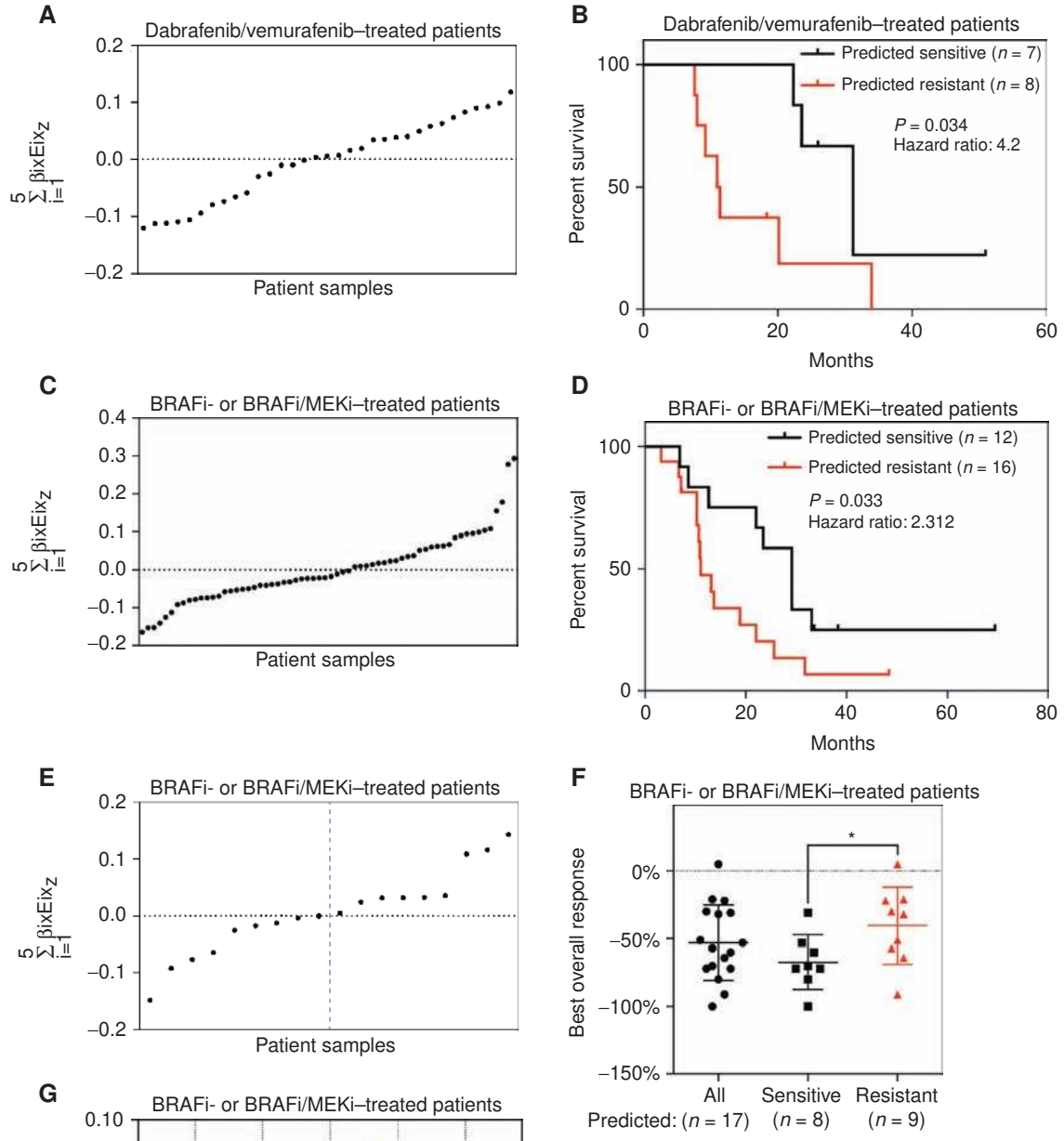

Figure 2. SOX10 addiction specifies sensitivity of BRAF-mutant melanomas to BRAF and MEK inhibitors in patients. **A,** Distribution of melanoma tumors resected from patients undergoing BRAFi therapy (35) based on the linear weighted sums of the individual gene expression values for each predictive feature. **B,** Kaplan–Meier plot of the overall survival of predicted targeted therapy–sensitive and –resistant dabrafenib/vemurafenib-treated patients with melanoma (35). Statistical significance was assessed using the log-rank (Mantel–Cox) test. **C,** Distribution of melanoma tumors resected from patients undergoing BRAFi/MEKi therapy based on the linear weighted sums of the individual gene expression values for each predictive feature. **D,** Kaplan–Meier plot of the overall survival of predicted targeted therapy–sensitive and –resistant vemurafenib- or dabrafenib/trametinib-treated patients with melanoma. Statistical significance was assessed using the log-rank (Mantel–Cox) test. **E,** Distribution of melanoma tumors resected from patients undergoing BRAFi/MEKi therapy (ref. 37; blue dashed line is the dichotomization boundary) based on the linear weighted sums of the individual gene expression values for each predictive feature. **F,** Best overall response of predicted targeted therapy–sensitive and –resistant vemurafenib- or dabrafenib/trametinib-treated patients with melanoma (ref. 37; two-sided unpaired Mann–Whitney test; *, $P = 0.0339$). **G,** Prediction scores of patient tumors isolated before (3A, 10A-2, 16A, 24A, 2A, and 7A) and on targeted therapy (vemurafenib or dabrafenib/trametinib; 3B, 10B-1, 16B, 24B, 2B, and 7B). Same numbers indicate tumors from same patients.

clones (Supplementary Fig. S5C and S5D), indicating a cancer cell–autonomous biomarker signature switch during the course of acquired resistance.

Nomination of TBK1 as a Therapeutic Target for Drug-Resistant Melanoma

Given the observed potential for predictive molecular discrimination of intrinsically BRAFi-sensitive and BRAFi-resistant melanoma together with the need to identify treatment strategies for patients harboring BRAFi-resistant tumors, we sought chemical leads with selective activity in the targeted therapy–resistant melanoma cell line cohort. To do this, we used the predictive feature set (linear weighted sums of each feature in each cell line) to stratify 35 melanoma cell lines for which whole-genome expression data were available together with experimentally defined or imputed IC_{50}s for 130 chemical compounds (ref. 32; Fig. 3A; Supplementary Fig. S6; Supplementary Table S12). Signal-to-noise (S2N) ratios were then calculated for each of these 130 compounds, according to their activity in the top 10% predicted BRAFi/MEKi-sensitive versus the top 10% predicted BRAFi/MEKi-insensitive cell lines, to identify any compounds with selective activity in the targeted therapy–resistant class (Supplementary Fig. S7A). BX795, a low nanomolar inhibitor of PDK1 (38) and the noncanonical IκB kinases TBK1 and IKKε (39), was the top hit (Fig. 3B). Differential toxicity of BX795 was first validated against 2 predicted sensitive cell lines (LOXIMVI and RPMI7951) and 2 predicted resistant cell lines (SKMEL28 and COLO792; Fig. 3C). To potentially disambiguate the mode of action underpinning the selective toxicity of BX795, we tested a 6-aminopyrazolopyrimidine (compound II) previously developed as a selective TBK1 inhibitor with no activity against PDK1 (40) as well as BX795 in a panel of 19 BRAF-mutant melanoma cell lines (Fig. 3D; Supplementary Fig. S7B). Although compound II was more potent in sensitive cell lines, these structurally distinct chemicals displayed highly correlated activity across the cell panel (Fig. 3E; Supplementary Fig. S7C, S7D, S7E, S7F, and S7G), suggesting that TBK1/IKKε-inhibitory activity is responsible for the cytotoxic phenotype. Consistent with this, MRT6737, a BX795 derivative that retains activity against TBK1 but not PDK1 (41), and momelotinib, a JAK1,2,3/TBK1/IKKε inhibitor, also exhibited similar dose-dependent selective toxicity profiles (Supplementary Fig. S7H and S7I). TBK1i-sensitive cell lines responded to inhibition of TBK1/IKKε activity by induction of apoptosis, suggesting these noncanonical IKK family members support context-selective cell survival signaling (Fig. 3F). Importantly, sensitivity to TBK1/IKKε inhibitors inversely correlated with both real and predicted sensitivity to trametinib (Fig. 3G, Supplementary Fig. S7J, S7K, S7L, and S7M). Taken together, these observations indicate selective vulnerability of vemurafenib/trametinib-resistant BRAF-mutant melanoma cells to inhibition of TBK1/IKKε activity. Notably, we found that A375 clones with acquired resistance to MEK inhibition were also sensitized to TBK1/IKKε inhibition in a manner predicted by their biomarker scores (Fig. 3H).

Within the discovery panel and the CCLE panel, we noted the presence of $BRAF^{WT}$ melanoma cell lines with biomarker signatures that were predictive of sensitivity to TBK1/IKKε inhibition (Fig. 1A; Supplementary Fig. S4C). Evaluation of 10 $BRAF^{WT}$ lines from across the cell line panel revealed significant concordance of BX795 and compound II sensitivity with the biomarker scores (Fig. 3I and J; Supplementary Fig. S7N). CHL1 was an unanticipated responder, with a biomarker score that predicted resistance to TBK1/IKKε inhibition (Fig. 3I). To search for an underlying discriminating feature associated with this response, we compared the whole-genome transcript profiles of TBK1i-sensitive (Hs895.T, Hs934.T, Hs839.T, and CHL1) and TBK1i-resistant (COLO729 and MEWO) $BRAF^{WT}$ melanoma cell lines. S2N analysis revealed selective downregulation of pigmentation genes and PGC1α, all MITF transcriptional targets, in TBK1i-sensitive cell lines (Supplementary Table S14), a correlation that was also observed in CHL1 (Fig. 3K). This indicates that the biomarker score has some false-negative associations that may be a consequence of similar cellular states that occur through different genetic or epigenetic alterations. Nevertheless, ROC curve analysis of actual versus predicted response to compound II of all tested melanoma cell lines ($N = 16$ from the discovery set, $N = 13$ from the CCLE set) suggests that the biomarker effectively detects distinct subtypes of melanoma that correspond to sensitivity or resistance to TBK1i (Fig. 3L).

To determine whether TBK1/IKKε vulnerability was detectable and actionable in heterogeneous melanoma tissues, we used the predictive feature set to stratify a cohort of molecularly annotated patient-derived xenografts (PDX; refs. 42–45) and tested the resulting predictions in short-term cultures derived from the corresponding PDX model (Supplementary Fig. S7O and S7P; Supplementary Table S12). Positive results in representative samples with both BX795 (Supplementary Fig. S7Q) and compound II (Supplementary Fig. S7R) indicated that predictable sensitivity patterns are conserved in this more physiologically relevant model.

Given the activity of TBK1/IKKε inhibition against $BRAF^{WT}$ melanoma cells, we considered potential activity in uveal melanoma (UVM). We used biomarker signature scores of < -0.1 and >0.1 to assign The Cancer Genome Atlas (TCGA) UVM samples into predicted TBK1i-resistant or TBK1i-sensitive cohorts, and found that the latter was associated with dismal prognosis (Supplementary Fig. S7S). We then ranked a panel of UVM cell lines using the same metric (Supplementary Fig. S7T). The two cell lines (MEL285 and MEL290) with biomarker expression scores predicting sensitivity to TBK1/IKKε inhibition were most responsive to both compound II and BX795 (Supplementary Fig. S7U–S7X) and nonresponsive to MEK inhibition (Supplementary Fig. S7Y and S7Z), and indicating mechanistic conservation of these cell states in cutaneous melanoma and UVM and that TBK1 is a potential intervention target in UVM with dismal prognosis.

TBK1/IKKε Addiction Is Conserved *In Vivo* and Corresponds to a Cell-Autonomous Innate Immune Melanoma Subtype

To test if TBK1/IKKε are targetable *in vivo*, we first examined the pharmacokinetics of compound II and BX795 in mice. Good aqueous solubility allowed compound II formulation in 100% saline, whereas BX795 required 10% DMSO and 10% cremophor. Effective peak serum concentrations

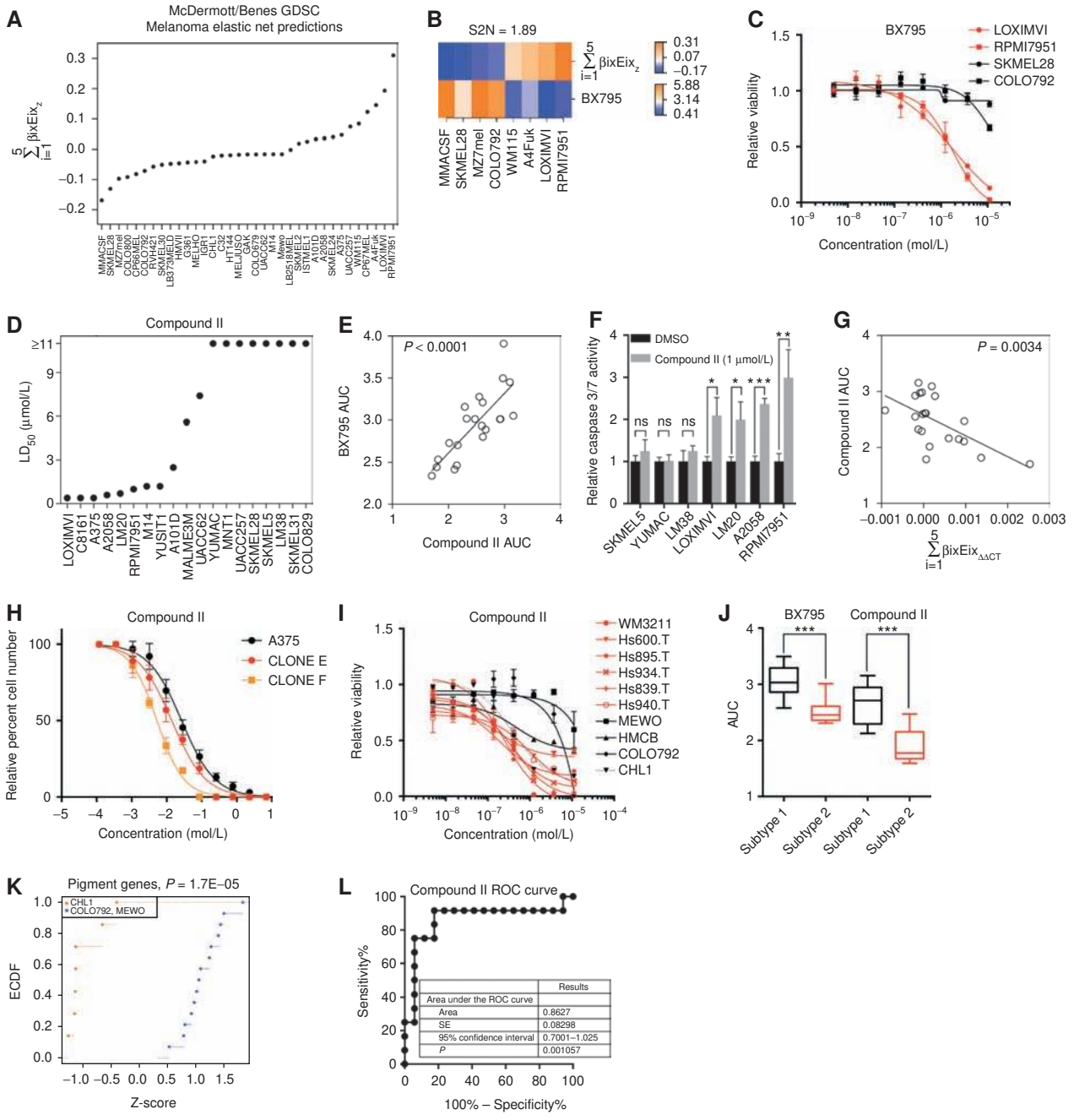

Figure 3. Nomination of TBK1 as a therapeutic target for drug-resistant melanoma. **A,** Distribution of 35 melanoma cell lines based on the linear weighted sums of the individual expression values for each predictive feature. **B,** S2N ratios identify BX795 IC_{50}s as corresponding to selective activity against predicted drug-resistant melanoma. Top row indicates prediction score. Second row indicates real and imputed IC_{50}s (log_{10} µmol/L) for BX795 toxicity in the indicated cell lines. **C,** BX795 dose–response curves for cell lines in Fig. 3B. **D,** Compound II LD_{50} values in the melanoma panel. **E,** Linear regression analysis of BX795 and compound II AUC values for each cell line in the melanoma panel. **F,** Caspase-3 and -7 activity was measured following exposure of TBK1 inhibitor–sensitive and –resistant cell lines to DMSO or compound II (1 µmol/L) for 24 hours. Bars indicate mean ± SD ($n = 3$). *, $P = 0.0132$ (LOXIMVI); *, $P = 0.0174$ (LM20); **, $P = 0.0076$; and ***, $P = 0.0002$, two-sided unpaired Student t test. **G,** Linear regression analysis of compound II AUC values for each cell line in the melanoma panel and the prediction scores determined using a summed-weight metric based on the elastic net–derived expression features. **H,** Compound II dose–response curves for A375 parental cells and A375 MEKi-resistant clones. Dots indicate mean ± SD ($n = 3$). **I,** Compound II dose–response curves for $BRAF^{WT}$ predicted TBK1i-sensitive (red) and -resistant (black) melanoma cell lines. **J,** Comparison of AUC values for dose–response curves from predicted TBK1i-resistant (subtype 1) and -sensitive (subtype 2) melanoma cell lines exposed to BX795 (two-sided unpaired Mann–Whitney test; ***, $P = 0.0001$) and compound II (two-sided unpaired Mann–Whitney test; ***, $P = 0.0002$). **K,** Cumulative distribution function (CDF) plot of mRNA expression of pigment genes (*MITF, DCT, TYR, MLANA, TYRP1, PMEL*, and *PPARGC1*) comparing TBK1 inhibitor–sensitive CHL1 and TBK1 inhibitor–resistant COLO792 and MEWO cell lines. $P = 1.7E-05$, one-sided two-sample Kolmogorov–Smirnov test. **L,** ROC curve analysis for compound II response. ECDF, empirical cumulative distribution function.

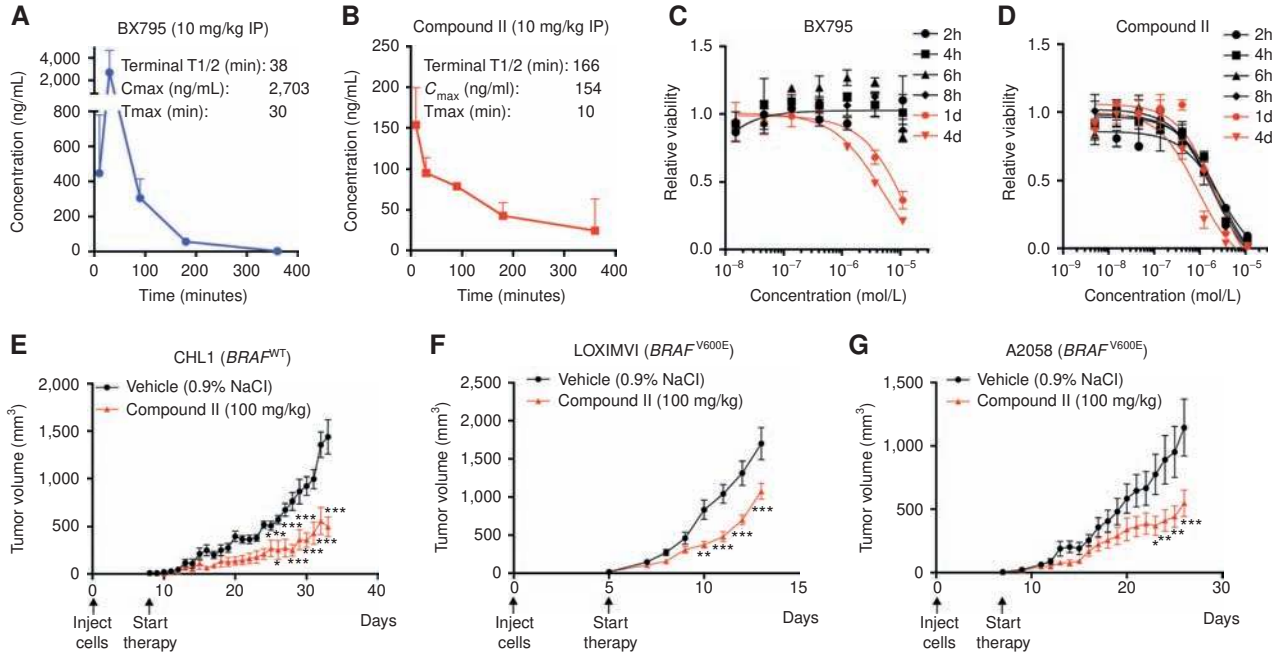

Figure 4. TBK1/IKKε addiction is conserved *in vivo*. **A** and **B,** Pharmacokinetic assays for BX795 (**A**) and compound II (**B**) indicate the maximum concentrations of the compounds in plasma, time to reach the maximum concentrations, and half-life of the compounds following i.p. injection at 10 mg/kg. **C** and **D,** LOXIMVI cells were exposed to BX795 (**C**) or compound II (**D**) at the indicated concentrations for the indicated times. Cell viability was measured after 96 hours for all conditions. Bars indicate mean ± SD ($n = 3$). **E–G,** 1×10^6 CHL1 cells (**E**), 5×10^5 LOXIMVI cells (**F**), or 7.5×10^5 A2058 cells/flank (**G**) were injected subcutaneously into one flank (CHL1) or both flanks (LOXIMVI and A2058) of NOD/SCID IL2Rγ^{null} (NSG) mice ($N = 8$ mice per group). Compound II (100 mg/kg) or saline were delivered i.p. daily after detection of palpable tumors (5 days after inoculation for LOXIMVI and 7 days after inoculation for A2058 and CHL1). Tumor volume versus treatment time is indicated. Dots indicate mean ± SEM ($N = 16$ for LOXIMVI and A2058, $N = 8$ for CHL1); *, $P = 0.0428$ (CHL1, day 24); *, $P = 0.0314$ (CHL1, day 26); **, $P = 0.0013$ (CHL1, day 27); **, $P = 0.0018$ (LOXIMVI); *, $P = 0.0324$ and **, $P = 0.0042$ (A2058, day 24); **, $P = 0.0017$ (A2058, day 25); and ***, $P < 0.0001$, two-way ANOVA followed by Bonferroni's multiple comparisons test.

(C_{max}) were achievable with both compounds; however, the terminal half-life ($T_{1/2}$) was under 40 minutes for BX795 and just under 3 hours for compound II (Fig. 4A and B). This indicated that IC_{50}s of compound II, as determined in culture, would be achievable in serum for a maximum of 2 to 3 hours after injection. Wash-out experiments, in cultured cells, suggested that a 2-hour exposure to compound II was sufficient to induce significant toxicity over the following 96 hours, which was not the case for BX795 (Fig. 4C and D). Given this, we elected to proceed with compound II for *in vivo* testing and developed an optimized chemical synthesis strategy to provide sufficient material (Supplementary Fig. S8A).

Two intrinsically MAPK pathway inhibitor–resistant BRAF^{V600E} melanoma cell lines, LOXIMVI and A2058, and the BRAF^{WT} melanoma cell line CHL1 were selected for xenograft studies. Upon presentation of palpable tumors, compound II was administered i.p. daily at 100 mg/kg. Despite the poor pharmacokinetic properties of compound II, in all cases, treatment with compound II significantly reduced growth of these aggressive tumors in mice as compared with the vehicle control (Fig. 4E–G). Compound II concentrations in resected tumors (2 hours after last dose) were measured by LC/MS-MS and found to be at or above the IC_{50} (Supplementary Fig. S8B). Current TBK1 inhibitors are not ideal for clinical use and will need to be developed into drug-like molecules to allow extensive preclinical modeling and potential use in patients. However, our results suggest that TBK1/IKKε inhibition may be a potential strategy for development of therapies to control BRAFi- and MEKi-resistant melanomas.

Recent molecular and pathophysiologic annotation of TCGA melanoma samples identified three major expression subtypes of melanoma with distinct patient outcomes: immune, keratin, and MITF^{lo} (46). To evaluate the relationship of these subtypes to predicted TBK1/IKKε addiction, we first ranked the TCGA melanoma tumor cohort based on our biomarker expression score (Fig. 5A). Tumors with high lymphocyte infiltration, as reported from patient sample histology, were excluded to reduce or eliminate any confounding contribution of immune cells to the quantitative gene expression score. Survival analyses with or without samples with high lymphocyte infiltration returned highly similar patient outcomes and indicated that the exclusion of tumors with high lymphocyte infiltration did not affect the reported TCGA expression subtype classification (Supplementary Fig. S9A and S9B) or distribution of mutation burden (Supplementary Fig. S9C). We found that the predicted TBK1i-sensitive subtype was significantly enriched within both the "immune" and "MITF^{lo}" TCGA-reported subtypes and de-enriched in the "keratin" subtype (Fig. 5B and C). Gene set enrichment analysis (GSEA) comparing samples from the tails of the prediction score distribution (prediction score cutoff <−0.05 and >0.05; Supplementary Fig. S9D) indicated that the predicted BRAFi/MEKi-sensitive

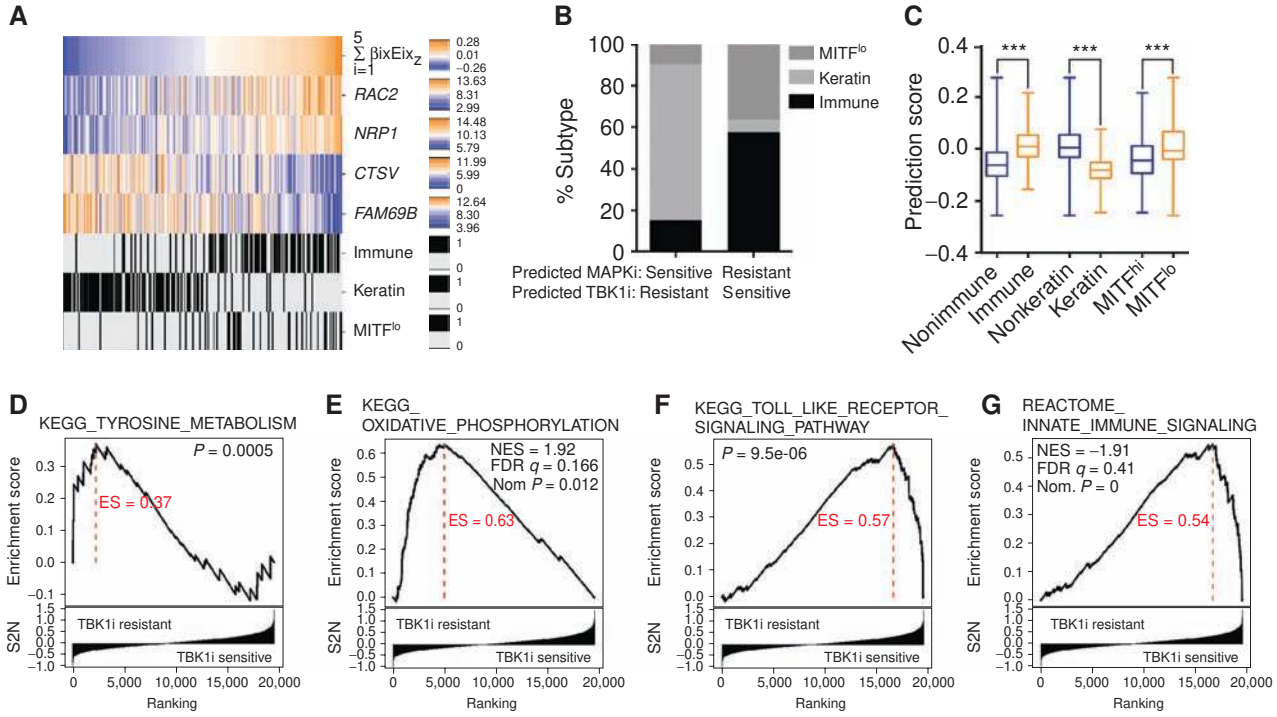

Figure 5. TBK1/IKKε addiction corresponds to a cell-autonomous innate immune melanoma subtype. **A,** Biomarker behavior in the TCGA skin cutaneous melanoma (SKCM) tumors with low lymphocyte infiltration. Top row indicates prediction score. Subsequent rows indicate $\log_2$-normalized expression of the indicated genes. Immune (black), keratin (black), and MITF-low (black) tumors are indicated as determined in The Cancer Genome Atlas Network (46). **B,** Bars indicate the percentage of different subtypes in predicted MAPKi-sensitive/TBK1i-resistant (prediction score cutoff is < −0.05) and predicted MAPKi-resistant/TBK1i-sensitive (prediction score cut-off is >0.05) subtypes. **C,** Comparison of prediction scores between the indicated subtypes; two-sided unpaired Mann–Whitney test, ***, $P < 0.0001$ for immune versus nonimmune and keratin versus non-keratin, ***, $P = 0.0009$ for MITF^{lo} versus MITF^{hi}. **D** and **E,** GSEA analysis shows a positive enrichment of tyrosine metabolism (**D**) and oxidative phosphorylation (**E**) in the predicted MAPKi-sensitive/TBK1i-resistant (prediction score cutoff is < −0.05) cohort. **F** and **G,** GSEA analysis shows a positive enrichment of toll-like receptor signaling (**F**) and innate immune signaling (**G**) in predicted MAPKi-resistant/TBK1i-sensitive (prediction score cutoff is >0.05) cohort.

subtype is enriched for tyrosine metabolism and oxidative phosphorylation, consistent with active SOX10 and MITF regulatory programs, whereas the predicted TBK1i-sensitive subtype is enriched for toll-like receptor and innate immune signaling (Fig. 5D–G). These cumulative observations support the notion that the predicted TBK1i-sensitive subtype is a mechanistically distinct "innate immune" pathway subtype that overlaps with previously identified melanoma subtypes (12, 47). Consistent with previous analyses of targeted therapy resistance, AXL mRNA and protein concentrations correlated with the "innate immune" subtype (Supplementary Fig. S9E and S9F); however, unlike TBK1 inhibitors, AXL inhibitors did not show preferential toxicity against cells in the "innate immune" subtype (47).

TBK1/IKKε Activates AKT and YAP to Support Survival of the Cell-Autonomous Immune Melanoma Subtype

Given the canonical participation of TBK1 in the cell autonomous innate immune/host defense signaling response, we evaluated TBK1 signaling in TBK1/IKKε inhibitor–resistant versus –sensitive subtypes. Accumulation of TBK1 with active site phosphorylation (serine 172) trended higher in the sensitive cohort, in both BRAF^{V600} and BRAF^{WT} cell lines, as compared with the resistant cohort, and correlated with significant enrichment of IFN-stimulated gene (ISG) expression (48), as would be expected downstream of TBK1/IKKε-dependent innate immune pathway activation (Fig. 6A–D; Supplementary Fig. S10A). We also measured IL6 and CCL5 secretion by ELISA and found that secretion of both cytokines was enriched in the innate immune subtype, consistent with persistent TBK1/IKKε signaling in that subtype (Supplementary Fig. S10B and S10C). AKT and NF-κB have both been implicated as direct targets of TBK1 survival signaling in cancer cells (40, 49, 50). Of interest, AKT activity was far more responsive to inhibition by compound II in the TBK1/IKKε-addicted cell lines (Fig. 6B). However, direct chemical inhibition of AKT (MK2206; ref. 51) or the canonical IκB kinases (IKK1/2, BMS-345541; ref. 52) had limited consequences on cell viability and no selectivity among cell lines tested (Supplementary Fig. S10D and S10E). Moreover, the PI3K inhibitors LY29400 and the PI3K and mTOR dual inhibitor BEZ235 did not display selective toxicity (Supplementary Fig. S10F and S10G), suggesting that modulation of these pathways is not sufficient to account for the selective toxicity of TBK1/IKKε inhibition. Moreover, perturbation of innate immune pathway components upstream and downstream of TBK1 by RNAi-mediated depletion (cGAS, STING,

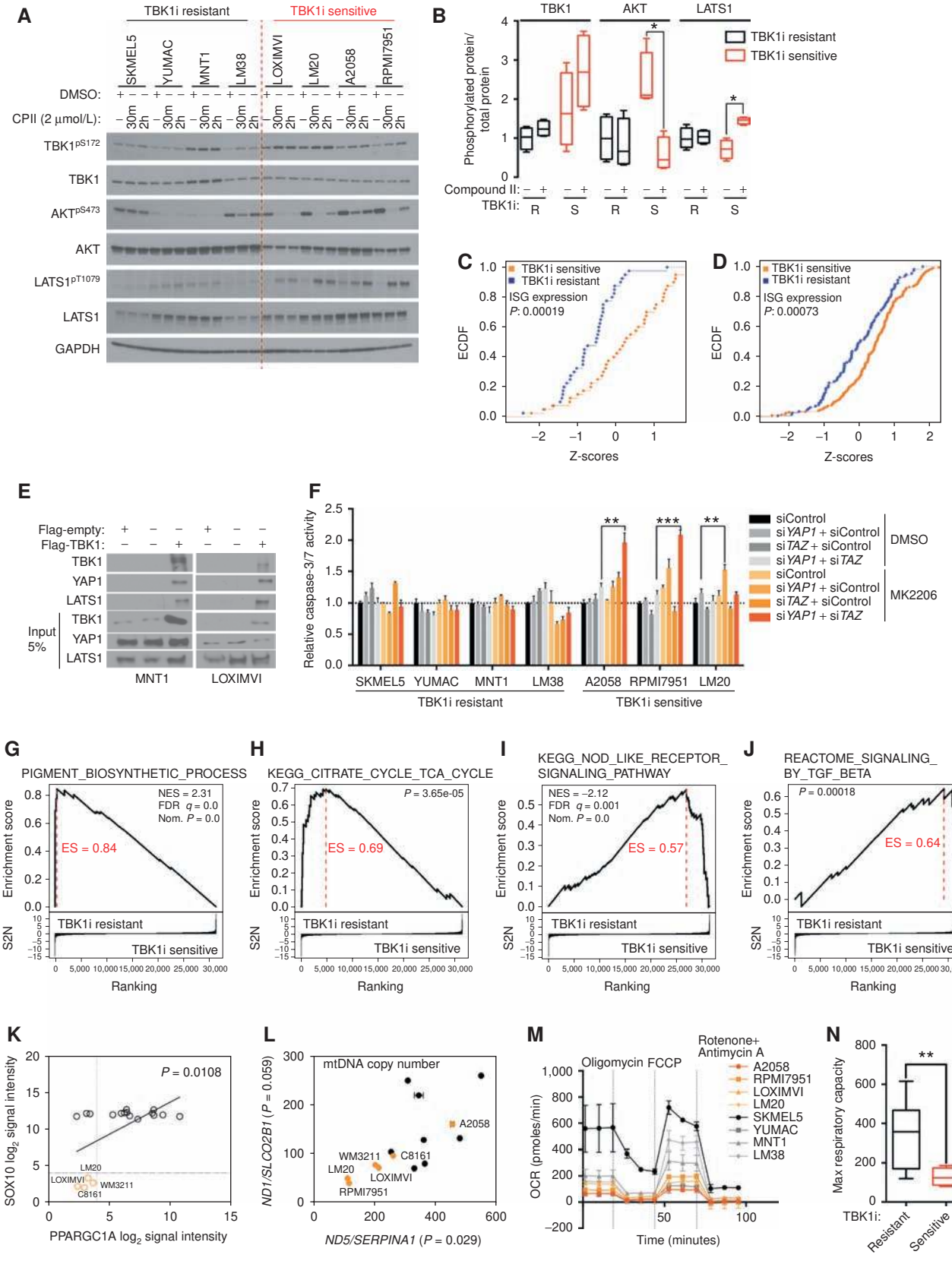

MAVS, and IRF3/IRF7; Supplementary Fig. S10H and S10I) or chemical-mediated inhibition (RIP1 kinase/necrostatin1; Supplementary Fig. S10J) also had no subtype-selective consequences on cell viability.

Of potential mechanistic significance, YAP pathway activation has recently been identified as a BRAFi resistance mechanism (53); inhibition of YAP activation has been reported upon shRNA-mediated *TBK1* depletion (54); and a physical association of TBK1 and Hippo pathway components has been suggested by proximity-mediated ligation assays (55). YAP activity is directly governed by the LATS1/2 tumor-suppressor kinases via inhibitory phosphorylation of YAP1 (56, 57). Notably, we found that compound II exposure selectively induced accumulation of activated LATS1 in the TBKi-sensitive cohort, suggesting TBK1 actively suppresses LATS1 in this setting (Fig. 6A and B; Supplementary Fig. S10A). In addition, epitope-tagged TBK1 immunoprecipitated together with endogenous YAP1 and LATS1, suggesting a physically proximal regulatory interaction (Fig. 6E). RNAi-mediated depletion of *YAP1* and its paralog *TAZ* greatly impaired the viability of LOXIMVI and CHL1, but was not sufficient to account for TBK1i-induced cytotoxicity for the majority of cell lines (Supplementary Fig. S10K and S10L). In contrast, combining YAP/TAZ depletion with AKT inhibition resulted in significant and selective induction of apoptosis in TBK1/IKKε-addicted cells (Fig. 6F). Thus, the mechanism of context-specific vulnerability to TBK1/IKKε inhibition is likely the combinatorial activation of the Hippo tumor-suppressor pathway together with suppression of AKT cell survival signaling.

Consistent with observations in TCGA tumor samples (Fig. 5D–G), and selective cell-autonomous innate immune pathway activation (Fig. 6A–C), comparison of the global gene expression profiles between BRAF/MEK-addicted versus TBK1/IKKε-addicted cell lines by GSEA returned pigment biosynthetic process and tricarboxylic acid (TCA) cycle as enriched in the BRAF/MEK-addicted subtype (Fig. 6G and H) versus NOD-like receptor signaling pathway and TGFβ signaling as enriched in the TBK1i-addicted subtype (Fig. 6I and J). Of note, PGC1α-associated oxidative phosphorylation is an acquired resistance mechanism observed in response to BRAF/MEK inhibitor exposure (58). Given the contrary de-enrichment of TCA cycle–associated gene expression in the TBK1/IKKε-addicted subtype, which is resistant to BRAF/MEK inhibition, we measured relative mitochondrial abundance by quantifying mitochondrial DNA copy number and mitochondrial function by measuring oxygen consumption rates in the BRAF/MEK-addicted subtype versus the TBK1/IKKε-addicted subtype. Consistent with the identification of PGC1α as a SOX10 transcriptional target (Supplementary Tables S6 and S9), the majority of TBK1/IKKε-addicted cell lines, which lack detectable SOX10 expression, were also lacking PGC1α expression (Fig. 6K; Supplementary Fig. S10M and S10N). These lines also displayed reduced mitochondrial DNA content (Fig. 6L) and significantly reduced oxygen consumption rates and maximum respiratory capacity as compared with the BRAF/MEK-addicted lines (Fig. 6M and N). These observations suggest the TBK1/IKKε-addicted "innate immune" subtype is a previously unrecognized, and mechanistically distinct, molecular subtype of melanoma that is refractory to current targeted therapy.

Distinct Epigenetic Cell Fate Programs Specify TBK1/IKKε Addiction

The distinct respiratory capacity among the BRAF/MEK-addicted versus TBK1/IKKε-addicted cells prompted us to investigate carbon utilization and cellular metabolite profiles. Stable isotope (^{13}C) tracing, using labeled glucose or glutamine, showed no detectable differences in the fractional contribution of ^{13}C to the downstream pools of TCA cycle intermediates among the cell lines (Supplementary Fig. S11). Lactate secretion was elevated in TBK1i-sensitive relative to TBK1i-resistant cell lines—consistent with elevated AKT activity and therefore increased glycolytic rates (Supplementary Fig. S12A) in the "innate immune" subtype; however, the respiring mitochondria in both subtypes displayed identical carbon utilization profiles. Moreover, exposure to TBK1/IKKε inhibitors did not detectably alter these profiles (Supplementary Fig. S11). By contrast, LC-MS/MS measurements of 141 intracellular metabolites revealed selective reduction of TCA cycle metabolic intermediates (α-ketoglutarate, aconitate, and aspartate) in TBK1i-sensitive cells upon compound II exposure for 2 hours (Supplementary Fig. S12B). This was correlated with accumulation of the polyamines putrescine and spermidine, which occurs upon perturbation of mitochondrial utilization of ornithine (refs. 59, 60; Supplementary Fig. S12C). Supporting mitochondrial TCA cycle activity by supplementation with dimethyl α-ketoglutarate significantly reduced compound II–induced apoptosis in sensitive cell lines (Supplementary Fig. S12D). Taken together,

Figure 6. TBK1/IKKε activates AKT and YAP to support survival of the cell-autonomous immune melanoma subtype. **A,** Whole-cell lysates, exposed to compound II for the indicated times, were assessed for the accumulation of the indicated phosphorylated proteins by immunoblot. **B,** Phosphorylated TBK1, AKT, and LATS1 protein concentrations relative to total TBK1, AKT, and LATS1 protein concentrations were measured from **A** using Image J (background corrected). *, $P = 0.0286$ (two-sided unpaired Mann-Whitney test). **C** and **D,** Cumulative distribution function (CDF) plot of mRNA expression of ISG expression comparing TBK1 inhibitor–sensitive and –resistant cell lines (**C**) and predicted TBK1 inhibitor–sensitive and –resistant TCGA SKCM tumors with low lymphocyte infiltration (**D**) one-sided two-sample Kolmogorov–Smirnov test. **E,** TBK1 was overexpressed in MNT1 and LOXIMVI, then immunoprecipitated with an antibody directed to the FLAG tag. Immunoprecipitates were analyzed for coprecipitation with YAP1 and LATS1. **F,** Caspase-3 and -7 activity was measured after exposure of MK2206 (1 μmol/L) for 24 hours following the siRNA-mediated knockdown of indicated genes in TBK1 inhibitor–sensitive and –resistant cell lines. Bars indicate mean ± SD ($n = 3$). **, $P = 0.0016$ (A2058); ***, $P < 0.0001$ (RPMI-7951); and **, $P = 0.0032$ (LM20), two-sided unpaired Student *t* test. **G** and **H,** GSEA analysis shows a positive enrichment of pigment biosynthetic process (**G**) and TCA cycle (**H**) in TBK1i-resistant cell lines. **I** and **J,** GSEA analysis shows a positive enrichment of nod-like receptor signaling (**I**) and TGFβ signaling (**J**) in TBK1i-sensitive cell lines. **K,** Linear regression analysis of SOX10 (*y*-axis) and PPARGC1A (*x*-axis) $\log_2$ signal intensity values from microarray in the melanoma discovery set. **L,** Dot plot shows the mitochondrial DNA copy number as measured by primer sets that designed for specific detection of two mitochondrial DNA targets (*ND1* and *ND5*) and two nuclear DNA targets (*SLCO2B1* and *SERPINA1*). **M,** Oxygen consumption rates (OCR) of TBK1 inhibitor–resistant (gray tones) and –sensitive (orange tones) cell lines. **N,** Maximum respiratory capacity in TBK1 inhibitor–sensitive and –resistant cell lines; two-sided unpaired Mann–Whitney test, **, $P = 0.0011$.

these observations indicate that although TBK1i-sensitive cells have mitochondria that respire "normally," there are fewer of them, and they are selectively sensitive to compound II exposure as compared with mitochondria in BRAFi/MEKi-sensitive counterparts (Supplementary Fig. S12C).

Unbiased evaluation of distinct baseline metabolic profiles in TBK1i-sensitive versus TBK1i-resistant cells, by S2N, revealed 1-methylnicotinamide (1-MNA) as the top-ranked molecule selectively enriched in the TBK1i-sensitive cell lines (Fig. 7A). We considered this to be of potential significance given that 1-MNA production by nicotinamide N-methyltransferase (NNMT) can globally inhibit histone methylation due to depletion of limiting pools of S-adenosyl methionine (61). In consequence, NNMT expression results in the accumulation of relaxed chromatin and is associated with epigenetic remodeling that supports the naïve pluripotent state of human embryonic stem cells (62) and promotes aggressively invasive tumorigenesis in a number of neoplastic disease lineages (61). Concordant with this relationship, we found that NNMT protein expression was exclusively detectable in the TBK1i-sensitive cells and was associated with global reduction in H3K27 trimethylation (Fig. 7B)—an EZH2-dependent epigenetic mark that otherwise promotes formation of repressive chromatin (63). siRNAs targeting *NNMT* expression selectively reduced viability of the TBK1i-sensitive cell lines, suggesting that persistent NNMT activity is apparently required to support this mechanistic subtype (Fig. 7C, two-sided unpaired Mann–Whitney test, $P = 0.004$). We considered that inhibition of the H3K27 methyltransferase EZH2 in TBK1i-resistant cells may generate a regulatory context that mimics NNMT expression and promotes addiction to TBK1/IKKε activity. Remarkably, we found that a 48-hour treatment with two different EZH2 inhibitors, with chemically distinct modes of action, was sufficient to sensitize three of the four TBK1i-resistant cell lines to compound II–induced programmed cell death (Fig. 7D; Supplementary Fig. S12E).

The above suggested that distinct molecular routes to melanomagenesis can result in at least two distinct regulatory states that specify differential dependence on RAF/MEK versus TBK1/IKKε survival signaling. Though not sufficient to serve as a predictive marker, a major distinguishing molecular feature for BRAF/MEK-addicted versus TBK1/IKKε-addicted subtypes is the selective presence of the lineage-specific transcription factor SOX10. We noted that among the direct gene targets of SOX10, which are suppressed by SOX10 expression, were multiple components of the TGFβ and innate immune regulatory networks (Supplementary Fig. S12F and S12G). Moreover, SOX10 expression indirectly suppressed expression of both NNMT and multiple components of the polycomb repressor complex 2 (which includes EZH2; Fig. 7E and F). These observations suggest that loss of SOX10 during neoplastic transformation from the neural crest lineage may account for many of the mechanistic features associated with the "innate immune" melanoma subtype we describe here. We noted that the "innate immune" melanoma lines consistently displayed elevated TGFβ target gene expression, with the exception of the outlier cases that responded poorly to TBK1/IKKε inhibitors (Fig. 7G and H; Supplementary Fig. S12H). Importantly, compensation with exogenous TGFβ was sufficient to sensitize these poor responders to compound II–induced apoptosis (Fig. 7I). Of note, mining of our previously reported functional signature ontology (FuSiOn) analysis of the human "kinome" (64) indicated a close mechanistic relationship between TGFBR2 and TBK1 (Supplementary Fig. S12I). We therefore asked if TBK1 itself may be activated by TGFβ. Short-term TGFβ stimulation resulted in a significant accumulation of TBK1 with active-site phosphorylation in the otherwise TBK1i-resistant cell lines. However, TBK1 status was unchanged by TGFβ in the TBK1i-sensitive cell lines, consistent with the presence of chronic TGFβ signaling (Fig. 7J–K). These observations suggest that a mechanistic consequence of melanomagenesis in the absence of SOX10 is both open chromatin and TBK1 activation (via TGFβ signaling), resulting in a tumorigenic state that is resistant to MEK inhibition but sensitive to TBK1/IKKε inhibition.

Finally, to help evaluate the breadth of the TBK1/IKKε-dependent regulatory network within the "innate-immune" subtype, we performed global quantitative mass spectrometric analysis of compound II–sensitive phosphoproteome in TBKi-sensitive versus TBKi-resistant cells. We employed a tandem mass tag (65) approach for quantitative evaluation of four cell lines (two compound II–sensitive and 2 compound II–resistant) exposed to carrier or TBK1i for 2 hours. We were able to identify and quantify a total of 31,820 phosphopeptides from this analysis (1% FDR), which corresponded to the identification of 8,897 unique, unambiguously localized phosphorylation sites, 2,210 of which were TBK1/IKKε

Figure 7. Distinct epigenetic cell fate programs specify TBK1/IKKε addiction. **A,** Comparison of 1-MNA abundance in TBK1 inhibitor–resistant (gray) and –sensitive cell lines (orange); two-sided unpaired Mann–Whitney test. TIC, total iron count. **B,** Whole-cell lysates were assessed for the accumulation of the indicated proteins by immunoblot. **C,** Dot plot shows compound II LD_{50} values (*y*-axis) and the consequence of NNMT depletion (*x*-axis) in the corresponding cell lines. **D,** Caspase-3 and -7 activity was measured after EZH2 inhibitor exposure (48 hours) in TBK1 inhibitor–resistant cell lines followed by the exposure to DMSO or compound II for an additional 24 hours. Bars indicate mean ± SD ($n = 3$). One-way ANOVA followed by Tukey multiple comparisons test; *, $P = 0.0106$ (SKMEL5); ***, $P = 0.0004$ [YUMAC, GSK126, and compound II (2.5 μmol/L)]; ***, $P = 0.006$ [YUMAC, EPZ-6438, and compound II (2.5 μmol/L)]; **, $P = 0.0025$ (LM38); and ***, $P < 0.0001$. **E,** Bars indicate the $\log_2$ fold change of the indicated genes in response to SOX10 depletion. **F,** Empirical cumulative distribution function (ECDF) plot of mRNA expression of histone methyltransferase activity-related genes in si*SOX10* (blue) versus the siControl-treated MNT1 cells (background). **G,** Illumina-derived $\log_2$ signal intensity values of indicated genes in TBK1 inhibitor–resistant (SKMEL5, YUMAC, MNT1, and LM38) and –sensitive (LOXIMVI, LM20, C8161, and WM3211) cell lines; two-sided unpaired Mann–Whitney test; **, $P = 0.008$ (TGFBR2); **, $P = 0.0015$ (SERPINE1); and **, $P = 0.0051$ (JUN). **H,** Affymetrix-derived $\log_2$ signal intensity values of SERPINE1 in TBK1 inhibitor–resistant (A101D, COLO829, and SKMEL31) and –sensitive (RPMI7951, LOXIMVI, Hs895.T, Hs839.T, Hs934.T, and Hs940.T) cell lines; two-sided unpaired Mann–Whitney test; *, $P = 0.0238$. **I,** Caspase-3 and -7 activity was measured after TGFβ stimulation (24 hours) in TBK1 inhibitor–resistant cell lines followed by the exposure to DMSO or compound II for an additional 24 hours. Bars indicate mean ± SD ($n = 3$). One-way ANOVA followed by Tukey multiple comparisons test; ***, $P < 0.0001$. **J,** Whole-cell lysates, stimulated with TGFβ for the indicated times, were assessed for the accumulation of the phosphorylated TBK1 by immunoblot. **K,** Fold difference of phosphorylated TBK1 protein concentrations at 30-minute timepoint relative to the 0-minute timepoint was measured from **J** using Image J (background corrected). **, $P = 0.0023$ (two-sided unpaired Mann-Whitney test).

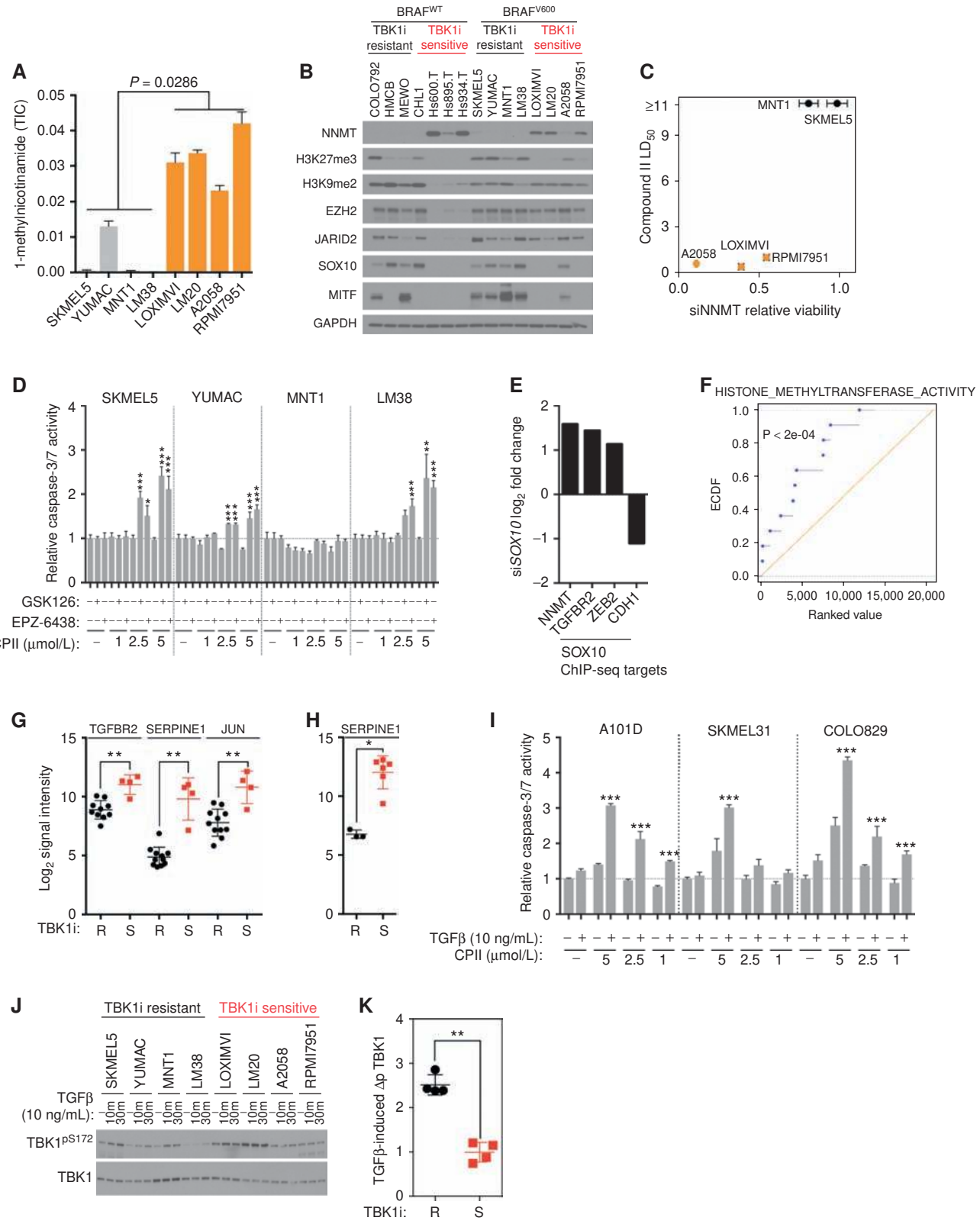

responsive in at least one cell line (fold change ≤ 0.5 or ≥ 2; Supplementary Table S15). Global comparison of compound II–sensitive events among the 4 lines indicated a close correlation of response specifically between cells of the "innate immune" subtype (Supplementary Fig. S12J and S12K). Among the most discriminatory changes were peptides corresponding to multiple proteins that participate in epigenetic regulation and a mesenchymal phenotype (Supplementary Fig. S12L). These context-dependent TBK1/IKKε substrates may therefore represent additional mechanistic components of a BRAF/MEK-insensitive melanomagenesis paradigm.

DISCUSSION

Cutaneous melanoma and lung squamous cell carcinoma (LSCC) share the distinction of harboring the highest mutational burdens among all human tumors (1, 2). However, in stark contrast to the dearth of recurrent somatic alterations in LSCC, fully half of melanomas possess recurrent variants of the *BRAF* oncogene (*BRAF*^{V600}; refs. 3, 4). In consequence, this seemingly monolithic mechanistic subtype has rightfully been the object of intense targeted therapy (66–69). The overall patient response frequency to targeted therapy is high (~50%; refs. 19, 70–72), yet intrinsic resistance and ready emergence of acquired resistance indicate that collateral genomic variation produces mechanistic diversity within the class of BRAF^{V600} tumors. Consistent with this notion, we identified a cohort of 15 different context-specific genetic vulnerabilities in melanoma cancer cell lines that are individually linked to distinct genomic features detectable in tumors from patients with melanoma (Supplementary Fig. S2A–S2C). Collectively, these target/biomarker relationships offer distinctive intervention strategies with potential relevance in approximately 20% of patients with melanoma.

Among the detected biomarker-associated vulnerabilities, addiction to the lineage-specific transcription factor SOX10 was strongly associated with genomic copy number–driven SOX10 gain of function in melanoma cancer cells and tumor samples. The stratification of melanoma cell lines based on SOX10 addiction led to the discovery of two mechanistic subtypes associated with distinct pharmacologic intervention opportunities and genomic features that can accurately assign subtype membership. The SOX10-dependent BRAF^{V600} subtype responds to clinical BRAF and MEK inhibitors. Notably, we found the SOX10-independent subtype is resistant to targeted therapy but also selectively sensitive to chemical inhibition of TBK1/IKKε kinase activity. Both subtypes can be simultaneously discriminated, from within melanoma cell line panels and melanoma patient cohorts, by a nearly bimodal 5-gene quantitative mRNA expression profile that is robust to measurement with multiple technical platforms. If verifiable in prospective human trials, these observations provide a path forward for biomarker-directed therapy by both predicting best responders to currently available MEK inhibitors and by detection of chemically targetable MEK-independent disease.

The host defense signaling kinases TBK1 and IKKε have been under consideration as oncology targets since 2006, but biological features predictive of response to TBK1/IKKε inhibitors have been lacking. Biomarker-positive, BRAF/MEK inhibitor–resistant melanoma now presents as an important therapeutic context for TBK1/IKKε inhibitors. Major tumorigenesis-associated TBK1/IKKε substrates include the innate immune transcription factors IRF3/7 (73, 74), the growth and survival kinases AKT and NF-κB, and the autophagy adaptor protein p62 (75). Elevated TBK1 activity within the targeted therapy–resistant/TBK1-dependent melanoma cohort was indicated by a qualitative enrichment of active site phosphorylation (T172) on TBK1 relative to total TBK1 protein and by a quantitative enrichment of IRF3/7 target gene expression. A context-selective biochemical response of biomarker-positive BRAF/MEK-independent melanoma cell lines to TBK1/IKKε inhibition was indicated by suppression of AKT pathway activation only in that subtype. However, direct chemical inhibition of AKT or NF-κB was not sufficient to recapitulate selective toxicity observed with TBK1/IKKε inhibitors.

Of note, shotgun proteomic discovery efforts have implicated TBK1 as a suppressor of Hippo pathway activation (54, 55). Moreover, the Hippo effector YAP has recently been demonstrated to promote resistance to RAF and MEK inhibition in multiple tumor types. Here, we found that Hippo pathway activity is generally low among all melanoma cell lines tested. However, the Hippo pathway was selectively activated by TBK1/IKKε inhibition in the TBK1/IKKε inhibitor–sensitive subtype. Furthermore, combined inhibition of AKT and YAP/TAZ activity selectively induced apoptosis in the TBK1/IKKε inhibitor–sensitive subtype. Therefore, we suspect that TBK1/IKKε likely supports melanoma cell survival by combined activation of AKT survival signaling and suppression of Hippo tumor-suppressor pathway activity. This combinatorial mechanism of action is likely preserved *in vivo* given the sensitivity of biomarker-positive xenograft tumors to systemic delivery of TBK1/IKKε inhibitors.

The TBK1/IKKε-sensitive cohort includes both BRAF-mutant and BRAF^{WT} tumors and corresponds to a gene expression phenotype reminiscent of host defense pathway activation and TGFβ-induced mesenchymal status. This expression signature was also enriched in melanoma tumors with low lymphocyte infiltration, suggesting that this phenotype corresponds to a mechanistically distinct melanoma subtype that we refer to as "innate immune." This subtype is enriched within both the "MITF^{lo}" and "immune" expression subtypes currently defined by TCGA efforts. As would be expected from the nature of the biomarker features, we found that high lymphocyte infiltration can confound detection of the "innate immune" subtype using ensemble gene expression measurements from patient samples—a limitation that we expect to overcome by development of IHC markers.

We find that mechanistic establishment of the "innate immune" melanoma cell state appears to be a consequence of relaxed chromatin and the ensuing release of TGFβ and host defense pathway activation. Importantly, artificially inducing this cell state by exposure to EZH2 inhibitors can be sufficient to establish TBK1/IKKε addiction in otherwise resistant melanoma cells. Remarkably, delineation of SOX10 target genes indicated that development of a melanomagenic program with or without SOX10 may play

a major role in determining BRAF/MEK versus TBK1/IKKε sensitivity, respectively. A key discriminatory mechanism appears to be SOX10-dependent suppression of NNMT and TGFBR2 expression. These two gene products collaborate within a feed-forward regulatory loop (61, 76, 77) to establish the relaxed chromatin, "mesenchymal" expression signature, and TBK1 pathway activation we observe within the "innate immune" subtype. As mentioned above, an additional functionally relevant component of the TBK1/IKKε-sensitive cell state is TBK1/IKKε-dependent YAP pathway activation. Though we, and others, can detect both physical and functional interactions between TBK1, LATS, and YAP1, we have not yet defined the mechanism by which TBK1/IKKε participates in Hippo pathway regulation. However, compelling observations in Drosophila (78), non–small cell lung cancer (79), and aggressive glioma (80) suggest that an interplay among mitochondrial damage (78), TGFβ-induced actin remodeling (81), and loss of PRC2 activity (79) can all generate cell states that are permissive to YAP activation.

In summary, we find that cell-based exploration of melanoma intervention opportunities can be a rich source for target discovery given sufficient resolution of molecular correlates that are preserved in patient populations. Here, these efforts have nominated new biomarker-coupled target opportunities for mechanistic subtypes of BRAF-mutant and $BRAF^{WT}$ melanomas, identified key elements within the SOX10 regulatory network required to support tumorigenicity, produced molecular predictors of best responders to $BRAF^{V600}$-targeted therapy, and delivered strategies to predict and chemically address nonresponders.

METHODS

Patient Samples

Written consent was obtained from all patients under approved Human Research ethics committee protocols from Royal Prince Alfred Hospital (Protocol X15-0454 and HREC/11/RPAH/444).

Cell Lines

Accurate provenance of all cell lines is followed using the PowerPlex 1.2 microsatellite detection kit (Promega) and fingerprint library maintained by the Minna/Gazdar laboratory and the ATCC. The ATCC performs DNA short-tandem repeat analysis to authenticate their cell line collection. Further in-house authentication was not performed for the cell lines obtained from the ATCC. In all experiments, each cell line was passaged less than 10 times. *Mycoplasma* testing of the cell lines was not performed. Primary melanoma cells from PDXs were kindly provided by Sean Morrison [University of Texas (UT) Southwestern Medical Center, Dallas, TX]. MNT1 cells were a kind gift from Michael Marks (University of Pennsylvania). LM17, LM17R, LM20, and LM38 were kind gifts from Monica Rodolfo (Fondazione IRCCS Istituto Nazionale Tumori, Milan, Italy). WM3211 cells were a kind gift from Meenhard Herlyn (Wistar Institute, Philadelphia, PA). WW165, YUMAC, and YUSIT1 were purchased from the Yale Skin Disease Research Center. LOXIMVI, M14, UACC257, UACC62, A375, MALME3M, SKMEL2, SKMEL5, and SKMEL28 were from NCI60 (National Cancer Institute, Bethesda, MD). A2058, RPMI7951, A101D, SKMEL31, COLO829, MEWO, HMCB, CHL1, Hs600.T, Hs895.T, Hs934.T, Hs839.T, and Hs940.T were purchased from the ATCC. COLO792 was purchased from Sigma-Aldrich. All cell lines were obtained between 2010 and 2016.

Mouse Xenograft Studies

Animals were cared for according to guidelines set forth by the American Association for Accreditation of Laboratory Animal Care and the U.S. Public Health Service policy on Human Care and Use of Laboratory Animals. All mouse studies were approved and supervised by the UT Southwestern Institutional Animal Care and Use Committee.

Small-Molecule Cell Viability Assays

For dose-response analyses, cells were first plated at a density of 1–2K/well in 96-well plates. Twenty-four hours after seeding, compounds solubilized in DMSO or DMSO alone (equal volume) were added to achieve the indicated final concentrations. Cell viability was measured 72 hours after compound exposure by CellTiter-Glo (Promega). Data were normalized using DMSO control–treated cells in the same plates. Response curves were modeled using a nonlinear regression curve fit with a three-parameter dose response using GraphPad Prism 6 software. AUC calculations were performed using the trapezoid rule by connecting every adjacent point defining the curve with a straight line and summing the areas below those points using GraphPad Prism 6 software. ROC AUC analysis was performed using GraphPad Prism 6 software. For ROC curve analysis, vemurafenib- or trametinib-treated cells were dichotomized (half and half) into "sensitive" or "resistant" bins based on the rank of their AUC values. Compound II– or BX795-treated cells were dichotomized based on the observed natural break of their LD_{50} values (i.e., Fig. 3D; Supplementary Fig. S7B).

Elastic Net Analysis

We employed a penalized linear regression model (elastic net) to select features that, either alone or in combination, can predict an siRNA viability response vector (82).

Candidate predictive features were selected from measures of gene expression (Illumina Bead arrays) across 19 cell lines. Measures were quantile normalized and background corrected with the MBCB package in R, and duplicated measurements for the same gene were compressed into a single value by taking the median value between the duplicates. Genes were included as candidate predictive features if they were expressed at a minimum $\log_2$ expression value of 6 in at least one cell line and if there was at least a 2-fold difference between minimal and maximal gene expression across the cell line panel, resulting in a total of 12,133 candidate genes.

Let $X \in \mathbb{R}^{nxp}$ be the matrix of predictive features where n is the number of cell lines included in the training dataset and p is the number of features, and let $y \in \mathbb{R}^n$ be the vector of binary sensitivity values for the same cell line panel. Columns of the predictive features matrix and y were normalized to have a mean of zero and an SD of 1. The elastic net attempts to find which weighted linear combination of the columns of the predictive features matrix can best approximate y, or it solves the following equation for w:

$$argmin_w \{\| y - Xw \|_2^2\}.$$

The elastic net solves the above by enforcing a penalty to the solution that makes the solution both unique and sparse so that only the features that best approximate y are left with nonzero weight values. It does this by combining L1-norm and L2-norm regularization parameters so that the elastic net formulation to the above problem is given by:

$$argmin_w \{\|y - Xw\|_2^2 + \lambda(\alpha \|w\|_2^2 + (1-\alpha)\|w\|_1)\}$$

where λ and α are two adjustable parameters such that λ controls the degree of the overall penalty and α controls the degree to which the L1-norm and L2-norm constraints are applied so that when α = 0, only the L1 penalty is applied and when α = 1, only the L2

penalty is applied. In order to determine the optimal values of alpha and lambda for the model, we carried out 100 iterations of 5-fold cross-validation where, for each iteration, cell lines were randomly resampled into different groups. The values of alpha and lambda were chosen to be those that resulted in the minimum mean squared error for each fold. Features were then chosen to be those with the highest weights that were selected as features in at least 80% of the cross-validation permutations.

Predicting Sensitivities in Test Sets

Weights were calculated for each of the features selected from the elastic net using the original 19 cell lines as a training set. Normalized predictive sensitivity values for untested samples (cell lines or tumor tissue) were then calculated for each of the samples in the test set with the following formula:

$$s_j = \sum_{i=1}^{n=5} w_i x_{ij}$$

where w_i is the weight determined from the elastic net for feature i, and x_{ij} is the normalized expression value of feature i in line j. The range of s_i values predicts the degree of sensitivity where a high value of s_i predicts resistant and a low value of s_i predicts sensitive. Melanoma discovery set: The described 5-gene SOX10 Elastic Net gene signature was used to generate prediction scores in 19 melanoma cells (Fig. 1A). mRNA expression data were from Illumina HT-12 V4 Beadchip microarrays. CCLE: The same 5-gene SOX10 Elastic Net gene signature was used to predict chemical and siRNA sensitivities in 61 melanoma cells from the CCLE panel (data available at www.broadinstitute.com/ccle). CCLE mRNA expression data were from Affymetrix HGU 133A Plus 2.0 microarrays. Garnett and colleagues (ref. 32; Fig. 3A and B; Supplementary Figs. S6 and S7A; Supplementary Table S12): Raw HTU 133A affymetrix expression data (.CEL files) from the McDermott/Benes GDSC dataset (32) were downloaded using ArrayExpress accession number E-MTAB-783. Data were background corrected with an RMA function and quantile normalized using the packages gcrma and affy in R. A 4-gene signature (FAM69B was not assayed in the array) was used to predict SOX10 sensitivity for 35 melanoma cell lines. TCGA cutaneous melanoma (Supplementary Fig. S5B; Supplementary Table S12): TCGA RNA-seq measures of RPKM gene expression were acquired for 80 UVM and for 333 Stage III Skin Cutaneous Melanoma (SKCM) tumor samples with manually curated high confidence clinical data using the cgdsr package in R. A 5-gene expression signature was used to predict tumor sensitivity to targeted therapies or TBK1i. Rizos and colleagues (ref. 35; Fig. 2A and B; Supplementary Table S12): Normalized and background corrected data (35) were downloaded using accession number GSE50509, representing dabrafenib- and/or vemurafenib-treated and untreated metastatic melanoma tumor samples from a total of 21 patients. Some tumors were assayed at multiple sites, resulting in 21 untreated samples and 33 compound treated tumor samples assayed with Illumina HT-12 V4 Bead Chip arrays. A 4-gene prediction expression signature (FAM69B was found to have poor dynamic range in this dataset and was removed from the signature) was used to predict targeted therapy sensitivity for treated and untreated tumor samples separately. Normalized and background corrected expression data were used to predict the targeted therapy sensitivity using a 5-gene biomarker from melanoma tumor samples isolated from patients treated with either $BRAF^{V600}$ therapy (dabrafenib/vemurafenib) or $BRAF^{V600}$ and MEKi combination therapy (dabrafenib and trametinib; Fig. 2C and D; Supplementary Table S13). Hugo and colleagues (ref. 37; Fig. 2E and F; Supplementary Table S12): RNA-seq–derived FPKM values were used to predict the targeted therapy sensitivity of 17 pretreatment tumors resected from patients undergoing dabrafenib, vemurafenib, or dabrafenib/trametinib therapy. Jonsson and colleagues (ref. 36; Supplementary Fig. S5A; Supplementary Table S12): Normalized and background corrected expression data assayed with Affymetrix HGU 133 Plus 2.0 arrays (36) were downloaded using GEO accession number GSE19234. A 5-gene expression signature was used to predict SOX10 sensitivity in 31 Stage IV metastatic melanoma tumor samples. Melanoma PDX (Supplementary Fig. S7O–S7P; Supplementary Table S12): Mouse xenograft–derived expression data assayed with Illumina HT-12 V4 Beadchip microarrays (45) were analyzed, representing a total of 81 xenografts from 32 patients. A 5-gene expression signature was used to predict TBK1 inhibitor sensitivity.

Survival Analysis

Differences in survival were calculated for the predicted targeted therapy–sensitive and –resistant classes represented by tails of the distributions. Cutoffs, defining the tails of the distributions, were specified by the inflection points of the predicted scores for each dataset. They are as follows: TCGA UVM: ± 0.1; TCGA SKCM: ± 0.05; GSE19234: ± 0.05; GSE50509: ± 0.05; Morrison PDX: ± 0.1. The Kaplan–Meier method was then used to estimate overall survival. The log-rank test was used to assess the statistical significance between the predicted targeted therapy–sensitive and -resistant groups. In addition, the log-rank analysis was used to generate HRs. All survival analyses were done using GraphPad Prism 6 software.

For further details, see Extended Experimental Procedures.

Disclosure of Potential Conflicts of Interest

R.J. Deberardinis is a consultant/advisory board member for Agios Pharmaceuticals. M.A. Davies reports receiving commercial research grants from AstraZeneca, Roche/Genentech, and Sanofi-Aventis, and is a consultant/advisory board member for Novartis, Roche/Genentech, and Sanofi-Aventis. J.A. Wargo has received honoraria from the speakers bureaus of Bristol-Myers Squibb, DAVA Oncology, and Illumina, and is a consultant/advisory board member for GlaxoSmithKline, Novartis, and Roche/Genentech. G.V. Long is a consultant/advisory board member for Amgen, BMS, Merck, and Novartis. No potential conflicts of interest were disclosed by the other authors.

Authors' Contributions

Conception and design: B. Eskiocak, E.A. McMillan, A. Zaman, L. Chin, M.A. White

Development of methodology: B. Eskiocak, E.A. McMillan, S. Mendiratta, M. Ding, Y. Yu, M.A. White

Acquisition of data (provided animals, acquired and managed patients, provided facilities, etc.): B. Eskiocak, C. Wang, M. Ding, A. Zaman, U. Eskiocak, M.P. Smith, J. Sudderth, R.J. Deberardinis, M.A. Davies, J.A. Wargo, Y. Yu, N.S. Williams, H. Rizos, G.V. Long, R. Kittler

Analysis and interpretation of data (e.g., statistical analysis, biostatistics, computational analysis): B. Eskiocak, E.A. McMillan, R.K. Kollipara, H. Zhang, M. Ding, M.P. Smith, J. Sudderth, K. Komurov, R.J. Deberardinis, C. Wellbrock, J.A. Wargo, Y. Yu, H. Rizos, R. Kittler, M.A. White

Writing, review, and/or revision of the manuscript: B. Eskiocak, E.A. McMillan, J.A. Wargo, Y. Yu, J.K. De Brabander, H. Rizos, G.V. Long, R. Kittler, M.A. White

Administrative, technical, or material support (i.e., reporting or organizing data, constructing databases): B. Eskiocak, C.G. Humphries, T.I. Rosales, J.K. De Brabander

Study supervision: B. Eskiocak, N.S. Williams, M.A. White

Other (performed synthesis of compound II): J. Garcia-Rodriguez

Other (performed synthesis, purification, and characterization of small-molecule TBK inhibitors): J.K. De Brabander

Other (supervised conduct of pharmacokinetic and metabolic stability studies in my laboratory and advised on dosing schedule to be used in animal studies conducted in senior author's laboratory based on this information): N.S. Williams
Other (collaborator with feedback on conception and design and data/materials contribution): L. Chin
Other (provided patient tissue samples and patient data and reviewed manuscript): G.V. Long

Acknowledgments

We thank Sean Morrison for providing the PDX samples and sharing transcript array data.

Grant Support

This study was supported by the Welch Foundation (I-1414, I-1422), the NIH (CA071443, CA176284, CA142543, CA093459), CPRIT (RP120718, RP110708), and the Kennedy Foundation. This study was also supported in part by the UT Southwestern Endowed Scholar Program, the Welch Foundation (I-1800), the NIH (GM114160), and the American Cancer Society (Research Scholar Grant, RSG-15-062-01-TBE) to Y. Yu. Y. Yu is a Virginia Murchison Linthicum Scholar in Medical Research and a CPRIT Scholar in Cancer Research.

The costs of publication of this article were defrayed in part by the payment of page charges. This article must therefore be hereby marked *advertisement* in accordance with 18 U.S.C. Section 1734 solely to indicate this fact.

Received August 30, 2016; revised December 7, 2016; accepted April 26, 2017; published OnlineFirst April 28, 2017.

REFERENCES

1. Alexandrov LB, Nik-Zainal S, Wedge DC, Aparicio SA, Behjati S, Biankin AV, et al. Signatures of mutational processes in human cancer. Nature 2013;500:415–21.
2. Lawrence MS, Stojanov P, Polak P, Kryukov GV, Cibulskis K, Sivachenko A, et al. Mutational heterogeneity in cancer and the search for new cancer-associated genes. Nature 2013;499:214–8.
3. Davies H, Bignell GR, Cox C, Stephens P, Edkins S, Clegg S, et al. Mutations of the BRAF gene in human cancer. Nature 2002;417:949–54.
4. Flaherty KT, Hodi FS, Fisher DE. From genes to drugs: Targeted strategies for melanoma. Nat Rev Cancer 2012;12:349–61.
5. Chapman PB, Hauschild A, Robert C, Haanen JB, Ascierto P, Larkin J, et al. Improved survival with vemurafenib in melanoma with BRAF V600E mutation. N Engl J Med 2011;364:2507–16.
6. Nazarian R, Shi H, Wang Q, Kong X, Koya RC, Lee H, et al. Melanomas acquire resistance to B-RAF(V600E) inhibition by RTK or N-RAS upregulation. Nature 2010;468:973–7.
7. Emery CM, Vijayendran KG, Zipser MC, Sawyer AM, Niu L, Kim JJ, et al. MEK1 mutations confer resistance to MEK and B-RAF inhibition. Proc Natl Acad Sci U S A 2009;106:20411–6.
8. Long GV, Fung C, Menzies AM, Pupo GM, Carlino MS, Hyman J, et al. Increased MAPK reactivation in early resistance to dabrafenib/trametinib combination therapy of BRAF-mutant metastatic melanoma. Nat Commun 2014;5:5694.
9. Shi H, Hugo W, Kong X, Hong A, Koya RC, Moriceau G, et al. Acquired resistance and clonal evolution in melanoma during BRAF inhibitor therapy. Cancer Discov 2014;4:80–93.
10. Johannessen CM, Boehm JS, Kim SY, Thomas SR, Wardwell L, Johnson LA, et al. COT drives resistance to RAF inhibition through MAP kinase pathway reactivation. Nature 2010;468:968–72.
11. Girotti MR, Pedersen M, Sanchez-Laorden B, Viros A, Turajlic S, Niculescu-Duvaz D, et al. Inhibiting EGF receptor or SRC family kinase signaling overcomes BRAF inhibitor resistance in melanoma. Cancer Discov 2013;3:158–67.
12. Sun C, Wang L, Huang S, Heynen GJ, Prahallad A, Robert C, et al. Reversible and adaptive resistance to BRAF(V600E) inhibition in melanoma. Nature 2014;508:118–22.
13. Wang J, Huang SK, Marzese DM, Hsu SC, Kawas NP, Chong KK, et al. Epigenetic changes of EGFR have an important role in BRAF inhibitor-resistant cutaneous melanomas. J Invest Dermatol 2015;135:532–41.
14. Abel EV, Basile KJ, Kugel CH 3rd, Witkiewicz AK, Le K, Amaravadi RK, et al. Melanoma adapts to RAF/MEK inhibitors through FOXD3-mediated upregulation of ERBB3. J Clin Invest 2013;123:2155–68.
15. Villanueva J, Vultur A, Lee JT, Somasundaram R, Fukunaga-Kalabis M, Cipolla AK, et al. Acquired resistance to BRAF inhibitors mediated by a RAF kinase switch in melanoma can be overcome by cotargeting MEK and IGF-1R/PI3K. Cancer Cell 2010;18:683–95.
16. Shi H, Moriceau G, Kong X, Lee MK, Lee H, Koya RC, et al. Melanoma whole-exome sequencing identifies (V600E)B-RAF amplification-mediated acquired B-RAF inhibitor resistance. Nat Commun 2012;3:724.
17. Poulikakos PI, Persaud Y, Janakiraman M, Kong X, Ng C, Moriceau G, et al. RAF inhibitor resistance is mediated by dimerization of aberrantly spliced BRAF(V600E). Nature 2011;480:387–90.
18. Flaherty KT, Robert C, Hersey P, Nathan P, Garbe C, Milhem M, et al. Improved survival with MEK inhibition in BRAF-mutated melanoma. N Engl J Med 2012;367:107–14.
19. Lito P, Rosen N, Solit DB. Tumor adaptation and resistance to RAF inhibitors. Nat Med 2013;19:1401–9.
20. Hodi FS, O'Day SJ, McDermott DF, Weber RW, Sosman JA, Haanen JB, et al. Improved survival with ipilimumab in patients with metastatic melanoma. N Engl J Med 2010;363:711–23.
21. Robert C, Thomas L, Bondarenko I, O'Day S, Weber J, Garbe C, et al. Ipilimumab plus dacarbazine for previously untreated metastatic melanoma. N Engl J Med 2011;364:2517–26.
22. Topalian SL, Hodi FS, Brahmer JR, Gettinger SN, Smith DC, McDermott DF, et al. Safety, activity, and immune correlates of anti-PD-1 antibody in cancer. N Engl J Med 2012;366:2443–54.
23. Hamid O, Robert C, Daud A, Hodi FS, Hwu WJ, Kefford R, et al. Safety and tumor responses with lambrolizumab (anti-PD-1) in melanoma. N Engl J Med 2013;369:134–44.
24. Cooper ZA, Juneja VR, Sage PT, Frederick DT, Piris A, Mitra D, et al. Response to BRAF inhibition in melanoma is enhanced when combined with immune checkpoint blockade. Cancer Immunol Res 2014;2:643–54.
25. Frederick DT, Piris A, Cogdill AP, Cooper ZA, Lezcano C, Ferrone CR, et al. BRAF inhibition is associated with enhanced melanoma antigen expression and a more favorable tumor microenvironment in patients with metastatic melanoma. Clin Cancer Res 2013;19:1225–31.
26. Shakhova O, Zingg D, Schaefer SM, Hari L, Civenni G, Blunschi J, et al. Sox10 promotes the formation and maintenance of giant congenital naevi and melanoma. Nat Cell Biol 2012;14:882–90.
27. Garraway LA, Widlund HR, Rubin MA, Getz G, Berger AJ, Ramaswamy S, et al. Integrative genomic analyses identify MITF as a lineage survival oncogene amplified in malignant melanoma. Nature 2005;436:117–22.
28. Kleopa KA, Sargiannidou I. Connexins, gap junctions and peripheral neuropathy. Neurosci Lett 2015;596:27–32.
29. Thies A, Moll I, Berger J, Wagener C, Brummer J, Schulze HJ, et al. CEACAM1 expression in cutaneous malignant melanoma predicts the development of metastatic disease. J Clin Oncol 2002;20:2530–6.
30. Sivan S, Suzan F, Rona O, Tamar H, Vivian B, Tamar P, et al. Serum CEACAM1 correlates with disease progression and survival in malignant melanoma patients. Clin Dev Immunol 2012;2012:290536.
31. Barretina J, Caponigro G, Stransky N, Venkatesan K, Margolin AA, Kim S, et al. The Cancer Cell Line Encyclopedia enables predictive modelling of anticancer drug sensitivity. Nature 2012;483:603–7.
32. Garnett MJ, Edelman EJ, Heidorn SJ, Greenman CD, Dastur A, Lau KW, et al. Systematic identification of genomic markers of drug sensitivity in cancer cells. Nature 2012;483:570–5.

33. Potts MB, McMillan EA, Rosales TI, Kim HS, Ou YH, Toombs JE, et al. Mode of action and pharmacogenomic biomarkers for exceptional responders to didemnin B. Nat Chem Biol 2015;11:401–8.
34. Kim HS, Mendiratta S, Kim J, Pecot CV, Larsen JE, Zubovych I, et al. Systematic identification of molecular subtype-selective vulnerabilities in non-small-cell lung cancer. Cell 2013;155:552–66.
35. Rizos H, Menzies AM, Pupo GM, Carlino MS, Fung C, Hyman J, et al. BRAF inhibitor resistance mechanisms in metastatic melanoma: Spectrum and clinical impact. Clin Cancer Res 2014;20:1965–77.
36. Jonsson G, Busch C, Knappskog S, Geisler J, Miletic H, Ringner M, et al. Gene expression profiling-based identification of molecular subtypes in stage IV melanomas with different clinical outcome. Clin Cancer Res 2010;16:3356–67.
37. Hugo W, Shi H, Sun L, Piva M, Song C, Kong X, et al. Non-genomic and immune evolution of melanoma acquiring MAPKi resistance. Cell 2015;162:1271–85.
38. Feldman RI, Wu JM, Polokoff MA, Kochanny MJ, Dinter H, Zhu D, et al. Novel small molecule inhibitors of 3-phosphoinositide-dependent kinase-1. J Biol Chem 2005;280:19867–74.
39. Bain J, Plater L, Elliott M, Shpiro N, Hastie CJ, McLauchlan H, et al. The selectivity of protein kinase inhibitors: A further update. Biochem J 2007;408:297–315.
40. Ou YH, Torres M, Ram R, Formstecher E, Roland C, Cheng T, et al. TBK1 directly engages Akt/PKB survival signaling to support oncogenic transformation. Mol Cell 2011;41:458–70.
41. Clark K, Peggie M, Plater L, Sorcek RJ, Young ER, Madwed JB, et al. Novel cross-talk within the IKK family controls innate immunity. Biochem J 2011;434:93–104.
42. Quintana E, Piskounova E, Shackleton M, Weinberg D, Eskiocak U, Fullen DR, et al. Human melanoma metastasis in NSG mice correlates with clinical outcome in patients. Sci Transl Med 2012;4:159ra49.
43. Quintana E, Shackleton M, Foster HR, Fullen DR, Sabel MS, Johnson TM, et al. Phenotypic heterogeneity among tumorigenic melanoma cells from patients that is reversible and not hierarchically organized. Cancer Cell 2010;18:510–23.
44. Quintana E, Shackleton M, Sabel MS, Fullen DR, Johnson TM, Morrison SJ. Efficient tumour formation by single human melanoma cells. Nature 2008;456:593–8.
45. Eskiocak U, Ramesh V, Gill JG, Zhao Z, Yuan SW, Wang M, et al. Synergistic effects of ion transporter and MAP kinase pathway inhibitors in melanoma. Nat Commun 2016;7:12336.
46. The Cancer Genome Atlas Network. Genomic classification of cutaneous melanoma. Cell 2015;161:1681–96.
47. Konieczkowski DJ, Johannessen CM, Abudayyeh O, Kim JW, Cooper ZA, Piris A, et al. A melanoma cell state distinction influences sensitivity to MAPK pathway inhibitors. Cancer Discov 2014;4:816–27.
48. West AP, Khoury-Hanold W, Staron M, Tal MC, Pineda CM, Lang SM, et al. Mitochondrial DNA stress primes the antiviral innate immune response. Nature 2015;520:553–7.
49. Buss H, Dorrie A, Schmitz ML, Hoffmann E, Resch K, Kracht M. Constitutive and interleukin-1-inducible phosphorylation of p65 NF-{kappa}B at serine 536 is mediated by multiple protein kinases including I{kappa}B kinase (IKK)-{alpha}, IKK{beta}, IKK{epsilon}, TRAF family member-associated (TANK)-binding kinase 1 (TBK1), and an unknown kinase and couples p65 to TATA-binding protein-associated factor II31-mediated interleukin-8 transcription. J Biol Chem 2004;279:55633–43.
50. Pomerantz JL, Baltimore D. NF-kappaB activation by a signaling complex containing TRAF2, TANK and TBK1, a novel IKK-related kinase. EMBO J 1999;18:6694–704.
51. Hirai H, Sootome H, Nakatsuru Y, Miyama K, Taguchi S, Tsujioka K, et al. MK-2206, an allosteric Akt inhibitor, enhances antitumor efficacy by standard chemotherapeutic agents or molecular targeted drugs in vitro and in vivo. Mol Cancer Ther 2010;9:1956–67.
52. Burke JR, Pattoli MA, Gregor KR, Brassil PJ, MacMaster JF, McIntyre KW, et al. BMS-345541 is a highly selective inhibitor of I kappa B kinase that binds at an allosteric site of the enzyme and blocks NF-kappa B-dependent transcription in mice. J Biol Chem 2003;278:1450–6.
53. Lin L, Sabnis AJ, Chan E, Olivas V, Cade L, Pazarentzos E, et al. The Hippo effector YAP promotes resistance to RAF- and MEK-targeted cancer therapies. Nat Genet 2015;47:250–6.
54. Kim JY, Welsh EA, Oguz U, Fang B, Bai Y, Kinose F, et al. Dissection of TBK1 signaling via phosphoproteomics in lung cancer cells. Proc Natl Acad Sci U S A 2013;110:12414–9.
55. Couzens AL, Knight JD, Kean MJ, Teo G, Weiss A, Dunham WH, et al. Protein interaction network of the mammalian Hippo pathway reveals mechanisms of kinase-phosphatase interactions. Sci Signal 2013;6:rs15.
56. Hao Y, Chun A, Cheung K, Rashidi B, Yang X. Tumor suppressor LATS1 is a negative regulator of oncogene YAP. J Biol Chem 2008;283:5496–509.
57. Huang J, Wu S, Barrera J, Matthews K, Pan D. The Hippo signaling pathway coordinately regulates cell proliferation and apoptosis by inactivating Yorkie, the Drosophila Homolog of YAP. Cell 2005;122:421–34.
58. Gopal YN, Rizos H, Chen G, Deng W, Frederick DT, Cooper ZA, et al. Inhibition of mTORC1/2 overcomes resistance to MAPK pathway inhibitors mediated by PGC1alpha and oxidative phosphorylation in melanoma. Cancer Res 2014;74:7037–47.
59. Martinelli D, Diodato D, Ponzi E, Monne M, Boenzi S, Bertini E, et al. The hyperornithinemia-hyperammonemia-homocitrullinuria syndrome. Orphanet J Rare Dis 2015;10:29.
60. Shimizu H, Maekawa K, Eto Y. Abnormal urinary excretion of polyamines in HHH syndrome (hyperornithinemia associated with hyperammonemia and homocitrullinuria). Brain Dev 1990;12:533–5.
61. Ulanovskaya OA, Zuhl AM, Cravatt BF. NNMT promotes epigenetic remodeling in cancer by creating a metabolic methylation sink. Nat Chem Biol 2013;9:300–6.
62. Sperber H, Mathieu J, Wang Y, Ferreccio A, Hesson J, Xu Z, et al. The metabolome regulates the epigenetic landscape during naive-to-primed human embryonic stem cell transition. Nat Cell Biol 2015;17:1523–35.
63. Kirmizis A, Bartley SM, Kuzmichev A, Margueron R, Reinberg D, Green R, et al. Silencing of human polycomb target genes is associated with methylation of histone H3 Lys 27. Genes Dev 2004;18:1592–605.
64. Potts MB, Kim HS, Fisher KW, Hu Y, Carrasco YP, Bulut GB, et al. Using functional signature ontology (FUSION) to identify mechanisms of action for natural products. Sci Signal 2013;6:ra90.
65. Erickson BK, Jedrychowski MP, McAlister GC, Everley RA, Kunz R, Gygi SP. Evaluating multiplexed quantitative phosphopeptide analysis on a hybrid quadrupole mass filter/linear ion trap/orbitrap mass spectrometer. Anal Chem 2015;87:1241–9.
66. Long GV, Stroyakovskiy D, Gogas H, Levchenko E, de Braud F, Larkin J, et al. Combined BRAF and MEK inhibition versus BRAF inhibition alone in melanoma. N Engl J Med 2014;371:1877–88.
67. Larkin J, Ascierto PA, Dreno B, Atkinson V, Liszkay G, Maio M, et al. Combined vemurafenib and cobimetinib in BRAF-mutated melanoma. N Engl J Med 2014;371:1867–76.
68. Robert C, Karaszewska B, Schachter J, Rutkowski P, Mackiewicz A, Stroiakovski D, et al. Improved overall survival in melanoma with combined dabrafenib and trametinib. N Engl J Med 2015;372:30–9.
69. Flaherty KT, Puzanov I, Kim KB, Ribas A, McArthur GA, Sosman JA, et al. Inhibition of mutated, activated BRAF in metastatic melanoma. N Engl J Med 2010;363:809–19.
70. Ahronian LG, Sennott EM, Van Allen EM, Wagle N, Kwak EL, Faris JE, et al. Clinical acquired resistance to RAF inhibitor combinations in BRAF-mutant colorectal cancer through MAPK pathway alterations. Cancer Discov 2015;5:358–67.
71. Meador CB, Pao W. Old habits die hard: Addiction of BRAF-mutant cancer cells to MAP kinase signaling. Cancer Discov 2015;5:348–50.
72. Jain P, Polliack A, Ravandi F. Novel therapeutic options for relapsed hairy cell leukemia. Leuk Lymphoma 2015:1–9.
73. Fitzgerald KA, McWhirter SM, Faia KL, Rowe DC, Latz E, Golenbock DT, et al. IKKepsilon and TBK1 are essential components of the IRF3 signaling pathway. Nat Immunol 2003;4:491–6.

74. Sharma S, tenOever BR, Grandvaux N, Zhou GP, Lin R, Hiscott J. Triggering the interferon antiviral response through an IKK-related pathway. Science 2003;300:1148–51.
75. Pilli M, Arko-Mensah J, Ponpuak M, Roberts E, Master S, Mandell MA, et al. TBK-1 promotes autophagy-mediated antimicrobial defense by controlling autophagosome maturation. Immunity 2012;37:223–34.
76. Chambers RC, Leoni P, Kaminski N, Laurent GJ, Heller RA. Global expression profiling of fibroblast responses to transforming growth factor-beta1 reveals the induction of inhibitor of differentiation-1 and provides evidence of smooth muscle cell phenotypic switching. Am J Pathol 2003;162:533–46.
77. Hsu S, Kim M, Hernandez L, Grajales V, Noonan A, Anver M, et al. IKK-epsilon coordinates invasion and metastasis of ovarian cancer. Cancer Res 2012;72:5494–504.
78. Ohsawa S, Sato Y, Enomoto M, Nakamura M, Betsumiya A, Igaki T. Mitochondrial defect drives non-autonomous tumour progression through Hippo signalling in Drosophila. Nature 2012;490:547–51.
79. Serresi M, Gargiulo G, Proost N, Siteur B, Cesaroni M, Koppens M, et al. Polycomb repressive complex 2 Is a Barrier to KRAS-driven inflammation and epithelial-mesenchymal transition in non-small-cell lung cancer. Cancer Cell 2016;29:17–31.
80. Bhat KP, Salazar KL, Balasubramaniyan V, Wani K, Heathcock L, Hollingsworth F, et al. The transcriptional coactivator TAZ regulates mesenchymal differentiation in malignant glioma. Genes Dev 2011;25:2594–609.
81. Cantelli G, Orgaz JL, Rodriguez-Hernandez I, Karagiannis P, Maiques O, Matias-Guiu X, et al. TGF-beta-induced transcription sustains amoeboid melanoma migration and dissemination. Curr Biol 2015; 25:2899–914.
82. Zou H, Hastie T. Regularization and variable selection via the elastic net. J R Statist Soc B 2005;67:301–20.